3-26-2004

Error analysis of continuous GPS position time series

Simon D. P. Williams

Yehuda Bock

Peng Fang

Paul Jamason

Rosanne M. Nikolaidis

See next page for additional authors

Authors

Simon D. P. Williams, Yehuda Bock, Peng Fang, Paul Jamason, Rosanne M. Nikolaidis, Linette Prawirodirdjo, Meghan Miller, and Daniel J. Johnson

Error analysis of continuous GPS position time series

Simon D. P. Williams
Proudman Oceanographic Laboratory, Bidston, UK

Yehuda Bock, Peng Fang, Paul Jamason, Rosanne M. Nikolaidis, and Linette Prawirodirdjo
Cecil H. and Ida M. Green Institute of Geophysics and Planetary Physics, Scripps Institution of Oceanography, La Jolla, California, USA

Meghan Miller and Daniel J. Johnson[1]
Department of Geology, Central Washington University, Ellensburg, Washington, USA

Received 13 August 2003; revised 14 January 2004; accepted 4 February 2004; published 26 March 2004.

[1] A total of 954 continuous GPS position time series from 414 individual sites in nine different GPS solutions were analyzed for noise content using maximum likelihood estimation (MLE). The lengths of the series varied from around 16 months to over 10 years. MLE was used to analyze the data in two ways. In the first analysis the noise was assumed to be white noise only, a combination of white noise plus flicker noise, or a combination of white noise plus random walk noise. For the second analysis the spectral index and amplitude of the power law noise were estimated simultaneously with the white noise. In solutions where the sites were globally distributed, the noise can be best described by a combination of white noise plus flicker noise. Both noise components show latitude dependence in their amplitudes (higher at equatorial sites) together with a bias to larger values in the Southern Hemisphere. In the regional solutions, where a spatially correlated (common mode) signal has been removed, the noise is significantly lower. The spectral index of the power law in regional solutions is more varied than in the global solutions and probably reflects a mixture of local effects. A significant reduction in noise can be seen since the first continuous GPS networks began recording in the early 1990s. A comparison of the noise amplitudes to the different monument types in the Southern California Integrated GPS Network suggests that the deep drill braced monument is preferred for maximum stability. *INDEX TERMS:* 1206 Geodesy and Gravity: Crustal movements—interplate (8155); 1208 Geodesy and Gravity: Crustal movements—intraplate (8110); 1244 Geodesy and Gravity: Standards and absolute measurements; 1294 Geodesy and Gravity: Instruments and techniques; 1299 Geodesy and Gravity: General or miscellaneous; *KEYWORDS:* GPS, time series analysis, uncertainty

Citation: Williams, S. D. P., Y. Bock, P. Fang, P. Jamason, R. M. Nikolaidis, L. Prawirodirdjo, M. Miller, and D. J. Johnson (2004), Error analysis of continuous GPS position time series, *J. Geophys. Res.*, *109*, B03412, doi:10.1029/2003JB002741.

1. Introduction

[2] As with many other geophysical phenomena, noise in GPS position time series can be described as a power law process [*Mandelbrot*, 1983; *Agnew*, 1992], or one with time domain behavior that has power spectrum of the form

$$P_x(f) = P_0 \left(\frac{f}{f_0}\right)^{\kappa}, \tag{1}$$

where f is the temporal frequency, P_0 and f_0 are normalizing constants, and κ is the spectral index [*Mandelbrot and Van Ness*, 1968]. Naturally occurring processes often have more power at low frequencies compared to higher frequencies and have negative indices ranging from $-3 < \kappa < -1$. Such nonstationary processes, including classical Brownian motion (or "random walk") with $\kappa = -2$ (or $P_x \propto 1/f^2$) are called "fractional Brownian motions." Stationary processes with $-1 < \kappa < 1$, including the special case of uncorrelated white noise ($\kappa = 0$, P is flat), are called "fractional Gaussian" processes. The special case of $\kappa = -1$ (or $P_x \propto 1/f$) called "flicker" noise is commonly observed in a wide variety of dynamical processes, including sunspot variability, the wobble of the Earth about its axis, undersea currents, and uncertainties in time measured by atomic clocks [*Gardner*, 1978; *Mandelbrot*, 1983].

[3] It is important to understand the noise content of GPS position data so that realistic uncertainties can be assigned

[1]Now at Department of Earth and Space Sciences, University of Washington, Seattle, Washington, USA.

0148-0227/04/2003JB002741$09.00

to parameters estimated from them. The assumption that the noise is purely white leads, for example, to grossly underestimated site rate uncertainties. *Zhang et al.* [1997] concluded that rate uncertainties were 3–6 times greater when the preferred white plus flicker noise model was used instead of the white noise only model. Likewise, *Mao et al.* [1999] concluded that their rate uncertainties were underestimated by as much as an order or magnitude if they neglected the correlated noise. The estimate of the standard error in rate is dependent upon several parameters of power law noise including the amplitude, spectral index, and sampling interval [*Williams*, 2003a]. It is clear that the assumed noise type greatly affects the resulting rate uncertainty, and so an important part of deriving crustal motion models from GPS data is to classify and quantify the noise components.

[4] While analyzing the noise in GPS time series is important for providing realistic parameter uncertainties, it does not provide a means for reducing that noise. However, classification of the noise components can provide clues as to the source of the noise and point to the right fields of research to help increase the accuracy and precision. For example, geodetic monument instability due to varying conditions of the anchoring media (e.g., soil, bedrock, buildings) is considered an important source of noise, thought to follow a random walk process [*Johnson and Agnew*, 1995]. Therefore some continuous GPS arrays have adopted very expensive deep drill braced monuments [*Wyatt et al.*, 1989] as the preferred approach to minimize this error source [e.g., *Bock et al.*, 1997; *Wernicke et al.*, 2000]. The new western North America Plate Boundary Observatory (PBO) [*Silver et al.*, 1999] is planning to install about 850 new continuous GPS monuments using the deep drill braced monument designed by F. Wyatt for SCIGN and adopted by other continuous GPS (CGPS) networks in this region. An error analysis of existing CGPS time series, some with histories of over a decade, can help to distinguish if these monuments are necessary, or whether other much less expensive solutions are sufficient.

[5] The presence of a spatially correlated, common mode, positioning error in GPS time series [*Wdowinski et al.*, 1997] has, to a certain extent, divided GPS time series analysis into two types, global and regional, which mirrors the global and regional nature of GPS networks. Where there is a network of sites with sufficiently small baseline distances, the common mode signal can be reduced either by the use of a filtering algorithm (also known as stacking) [*Wdowinski et al.*, 1997] or by the use of a regional reference frame and daily Helmert transformations [e.g., *Hurst et al.*, 2000]. In the case of a globally distributed set of sites the baseline distances are generally so large that the sites are considered to be uncorrelated from each other. The common mode noise cannot therefore be reduced, and the noise in the series is typically higher than for regional networks [*Mao et al.*, 1999].

[6] The work presented here follows from previous studies in this field. The time between this study and those previous studies has allowed us to collect longer time series, a recognized shortcoming in the previous work. In addition, we have attempted to analyze a greater number of sites, both global and regional, from several different GPS solutions to hopefully gain a bigger insight into the nature of the noise components.

2. Previous Work

[7] *Zhang et al.* [1997] examined 19 months of continuous GPS (CGPS) data from 10 sites in southern California. A common mode signal was removed from the position time series so the results were for a regional network. Using maximum likelihood estimation (MLE) with integer spectral indices, *Zhang et al.* [1997] found that the noise in the data was best described as a combination of white noise and flicker noise. Using the power spectra, the noise was characterized by a fractal noise process with spectral index of −0.4. *Mao et al.* [1999] examined 3 years of data from a global distribution of 23 CGPS sites. Using both MLE at integer spectral indices and power spectra, they concluded that white noise plus flicker noise best described the noise content of the time series. A latitude dependence was found for the white noise part of the vertical component. Three permanent GPS sites in Europe were analyzed by *Calais* [1999]. A combination of white noise and flicker noise was the preferred model. Higher-frequency (1–30 s) GPS position time series have also been shown to contain white noise plus flicker noise [*Bock et al.*, 2000; J. Langbein and Y. Bock, High-rate real-time GPS network at Parkfield: Utility for detecting fault slip and seismic displacements, submitted to *Geophysical Research Letters*, 2004]. Several studies also acknowledge the importance of random walk noise in GPS data. Cumulative disturbances from the soils and weather displace geodetic monuments with respect to the deeper crust [*Johnson and Agnew*, 1995; *Langbein and Johnson*, 1997]. Whether or not the random walk noise is detectable depends on the length of the time series, the sampling frequency, and the relative amplitudes of the other noise components. Random walk noise has been identified in continuous strainmeter data [*Wyatt*, 1982, 1989; *Wyatt et al.*, 1989] and two-color electronic distance meter data [*Langbein and Johnson*, 1995], as well as very short baseline (50 m) GPS data from Piñon Flat Observatory (PFO) [*Johnson and Agnew*, 2000]. Random walk amplitudes can be as high as 3 mm/yr$^{1/2}$ for some geodetic data [*Johnson and Agnew*, 1995]. However, this type of disturbance can be mitigated by carefully designed monuments, like those GPS stations deployed in southern California in which the base is securely anchored at depth, laterally braced, and decoupled from the surface [*Wyatt et al.*, 1989; *Bock et al.*, 1997]. With this type of monument, for example, the random walk amplitude for the 50 m PFO baseline is only 0.4 mm/yr$^{1/2}$ [*Johnson and Agnew*, 2000]. However, regional GPS networks have much longer interstation spacings so that other sources of error such as known random atmospheric propagation effects [*Williams et al.*, 1998] could dominate the error budget.

3. Data

[8] In this study we analyze both global and regional time series of site positions. In addition, instead of restricting ourselves to data from just one analysis approach we chose to investigate several different data sets that were processed by

Table 1. Summary of the Nine GPS Solutions Used in This Study

Solution	Reference	Software Package	Start Date	Stop Date	Number of Sites in Solution	Number of Sites Used	Average Length, years	Maximum Length, years
SOPAC global	*Nikolaidis* [2002]	GAMIT/GLOBK	20 Jan. 1991	12 Jan. 2002	600	207	3.6	10.7
SOPAC SCIGN	*Nikolaidis* [2002]	GAMIT/GLOBK	20 Jan. 1991	12 Jan. 2002	221	147	2.7	10.7
JPL global (SCIGN_1.0.0)	*Zumberge et al.* [1997]	GIPSY/OASIS II	22 Jan. 1991	28 April 2002	>500	268	2.5	9.8
JPL SCIGN (SCIGN_2.0.0)	*Hurst et al.* [2000]	GIPSY/OASIS II	Jan. 1998	April 2000	127	58	2.2	2.2
USGS SCIGN	http://pasadena.wr.usgs.gov/	GAMIT/GLOBK	July 1997	June 2001	231	112	2.5	3.9
PANGA PANGA	*Miller et al.* [2001]	GIPSY/OASIS II	Jan. 1998	Dec. 2001	58	54	3.9	3.9
SOPAC PANGA	http://sopac.ucsd.edu/	GAMIT/GLOBK	Sept. 1992	March 2003	43	30	4.4	10.5
SOPAC BARGEN	http://sopac.ucsd.edu/	GAMIT/GLOBK	Aug. 1996	March 2003	47	47	4.7	6.6
REGAL REGAL	*Calais et al.* [2000]	GAMIT/GLOBK	Jan. 1996	July 2001	31	31	4.0	5.5

different analysis groups, with a mix of different software packages and different processing strategies. A summary of the nine GPS solutions described in this paper is given in Table 1.

[9] Figure 1 shows the distribution of sites used in this analysis and the number of solutions in which sites appear. The overlap of some sites in different solutions allows us to compare results between global and regional networks and between solutions. In total, there are 414 separate sites used in this analysis, of those 57 appear in five solutions, 32 in four solutions, 51 in three, and 115 in just two. The other 158 sites appear in just one solution. All of the sites that appear in four or more solutions are in California, and all but one of these, QUIN, are in southern California. An example of a time series for a site, FVPK, for which there are five solutions is given in Figure 2. FVPK is located in the margin of a basin undergoing uplift and subsidence due to groundwater pumping effects [*Bawden et al.*, 2001; *Watson et al.*, 2001] and is therefore subjected to large nonlinear deformation signals in both the horizontal and vertical. While the background deformation appears similar in all five solutions, the noise is evidently different in each.

3.1. SOPAC Reanalysis Global Solution

[10] In mid-1999, the Scripps Orbit and Permanent Array Center (SOPAC) began an extensive reanalysis of more than a decade of continuous GPS observations [*Nikolaidis*, 2002]. The daily site coordinates were estimated from the GPS measurements using the GAMIT software, version 9.94 (and 10.01) [*King and Bock*, 2000], and the GLOBK software, version 5.04 [*Herring*, 2000a]. A distributed network processing strategy [*Zhang*, 1996] was used with up to 48 sites per network. To obtain station coordinates in the International Terrestrial Reference Frame (ITRF) 1997, an adjustment was performed, using GLOBK's GLORG module, constraining the ITRF1997 coordinates and velocities of appropriate global tracking sites that compose the reference network. The particular set of stations used to define the global refer-

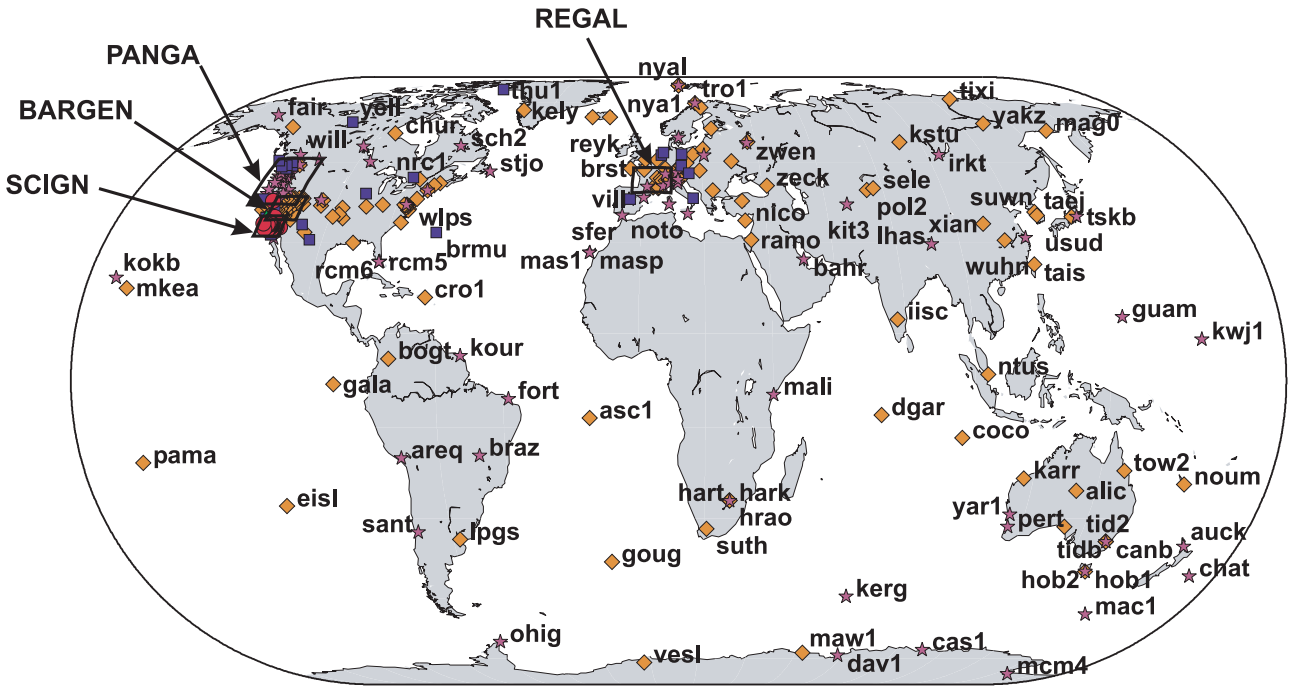

Figure 1. Map of the 414 sites used in this study. The boxes indicate the spatial extent of the four regional networks used. Sites marked with a diamond appear in only one solution, a star in two solutions, a square in three solutions, a triangle in four solutions, and a circle in five solutions.

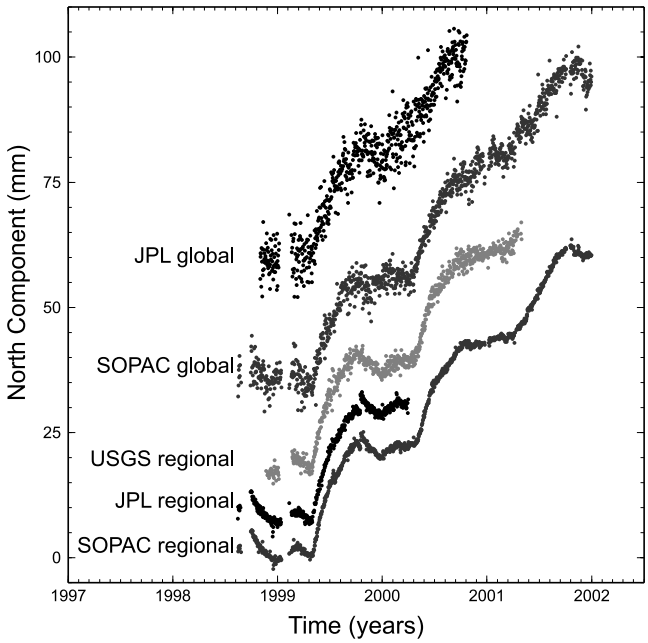

Figure 2. Time series for the north component of the SCIGN site FVPK from five individual GPS solutions (named). Each series is arbitrarily offset for clarity.

ence frame was chosen to provide optimal stability over the entire reanalysis period.

3.2. SOPAC Reanalysis SCIGN Regional Solution

[11] GPS observations from the Southern California Integrated GPS Network (SCIGN) (Figure 3b) were included in the SOPAC reanalysis described above and provide globally referenced topocentric north, east, up (NEU) position time series. The regional solution differed from the global solution by some additional steps. First, a common mode error signal was computed as the daily weighted mean of the residual noise from a set of regional fiducial sites [*Wdowinski et al.*, 1997]. With the goal of maintaining optimal reference frame stability over the 11-year analysis interval, the regional fiducial sites were chosen to be those with the earliest observation history. These are eight sites of the Permanent GPS Geodetic Array (PGGA), a forerunner to SCIGN [*Bock et al.*, 1993, 1997]: PIN1, PIN2, ROCH, JPLM, GOLF (combined GOLD and GOL2), SIO3 (combined SIO1, SIO2, and SIO3), VNDP, and MOJM. Second, postseismic exponential decays and/or rate changes were modeled at sites within a certain distance of large earthquakes (Joshua Tree, Northridge, Landers, Hector Mine). The above steps formed an iterative process and included the MLE error analysis described in this paper.

3.3. Jet Propulsion Laboratory SCIGN_1.0.0 Global Solution

[12] The Jet Propulsion Laboratory (JPL) daily global solution spans the 10-year period from 22 January 1991 to 28 April 2001. The data were processed using the point-processing strategy in the GIPSY-OASIS II software [*Zumberge et al.*, 1997].

3.4. JPL SCIGN_2.0.0 Regional Solution

[13] In addition to the SCIGN_1.0.0 solution, JPL also provides a regional solution for the SCIGN network that uses a regional reference frame to reduce the noise in station coordinates. The SCIGN_2.0.0 solution [*Hurst et al.*, [2000] used fixed precise GPS orbits and clocks in a precise point-positioning mode, followed by double difference ambiguity resolution and subsequent transformation into a regional definition of the ITRF1997 using a Helmert transformation.

3.5. U.S. Geological Survey Rapid Analysis SCIGN Regional Solution

[14] The U.S. Geological Survey (USGS) Pasadena office provides a rapid analysis solution of daily site coordinates for the SCIGN network. The data are processed using the GAMIT/GLOBK software, and the processing is initiated 7 hours after the end of each UTC day. The analysis used predicted IGS orbits, and the data were processed in several subregions, which were then combined in GLOBK. A common mode bias was removed by performing a seven-parameter transformation in the GLORG module of the GLOBK software. A total of 37 SCIGN sites were used to redefine the reference frame origin.

3.6. PANGA Regional Solution

[15] The analysis procedures used in the Pacific Northwest Geodetic Array (PANGA) [*Miller et al.*, 1998] (Figure 3a) are described by *Miller et al.* [2001]. The data were processed using GIPSY/OASIS II software using the precise point-positioning technique, and JPL generated fiducial free orbit solutions. Common mode signals were removed from all sites using the method described by *Wdowinski et al.* [1997]. The residuals from sites ALBH, CABL, DRAO, GOBS, PABH, and QUIN were used to form the common mode signal.

3.7. SOPAC PANGA Regional Solution

[16] SOPAC adopted the methodology of *Nikolaidis* [2002] for its weekly production of daily GPS position time series, as well as updating the underlying reference frame to ITRF2000 [*Altamimi et al.*, 2002]. The GPS data from the PANGA array were processed as part of SOPAC's production solutions. Unlike the SCIGN solution described in section 3.2, which used just eight sites with a long observation history to compute the common mode error, all reasonable sites in the PANGA array were used, that is, sites that are sufficiently long and considered to be stable.

3.8. SOPAC BARGEN Regional Solution

[17] The GPS data from the Basin and Range Geodetic Network (BARGEN) [*Davis et al.*, 2003] in the western United States (Figure 3c) are also processed with respect to ITRF2000 as part of the SOPAC weekly production solutions of daily GPS position time series. As for the SOPAC PANGA solution, all reasonable sites were used to form the common mode error, which was then removed from the individual time series.

3.9. REGAL Regional Solution

[18] The GPS data from the REGAL [*Calais et al.*, 2000] network in the western Alps (Figure 3d) were processed with the GAMIT/GLOBK software along with data from 10 global IGS stations to serve as ties to

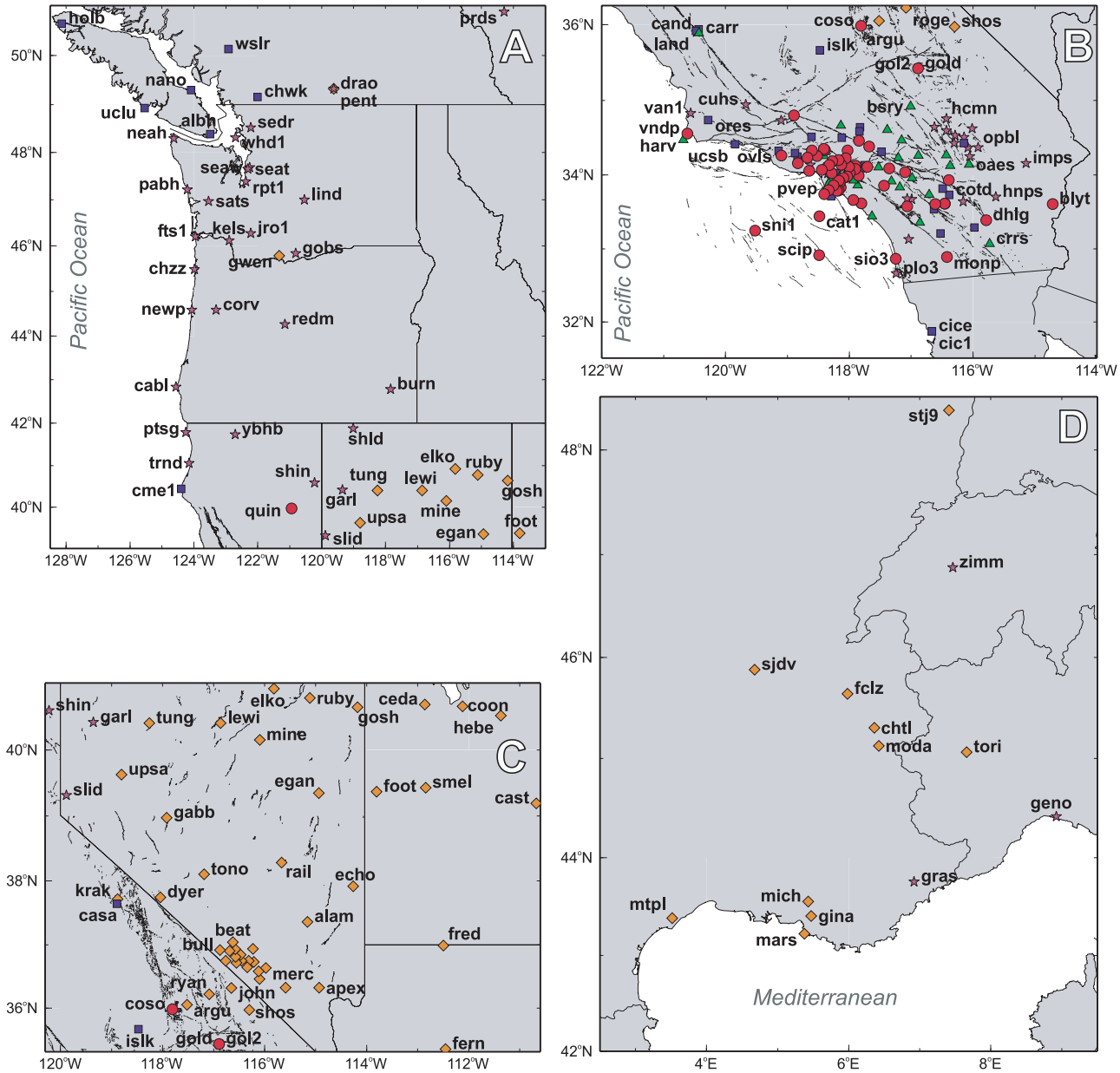

Figure 3. Maps of the sites used in the study from the regional GPS solutions for (a) PANGA array, (b) SCIGN array, (c) BARGEN array, and (d) REGAL array. Symbols for sites are the same as in Figure 1.

ITRF97. The processing scheme is described by *Calais et al.* [2000].

4. Maximum Likelihood Estimation

[19] We used maximum likelihood estimation (MLE) as described by *Langbein and Johnson* [1997], *Zhang et al.* [1997], and *Mao et al.* [1999] in order to measure the amounts of white noise and power law (flicker, random walk) noise in the time series. To allow the consideration of a wider range of power law processes, MLE is also used here to establish an overall power law noise model that best describes the data. To estimate noise components using MLE, the probability function is maximized by adjusting the data covariance matrix. Therefore

$$\mathrm{lik}(\hat{\mathbf{v}}, \mathbf{C}) = \frac{1}{(2\pi)^{N/2}(\det \mathbf{C})^{1/2}} \exp\left(-0.5\hat{\mathbf{v}}^{\mathbf{T}}\mathbf{C}^{-1}\hat{\mathbf{v}}\right), \qquad (2)$$

where lik is likelihood and det is the determinant of a matrix, or if we take the natural logarithm,

$$\mathrm{MLE} = \ln[\mathrm{lik}(\hat{\mathbf{v}}, \mathbf{C})] = -\frac{1}{2}\left[\ln(\det \mathbf{C}) + \hat{\mathbf{v}}^{\mathbf{T}}\mathbf{C}^{-1}\hat{\mathbf{v}} + N\ln(2\pi)\right], \qquad (3)$$

where ln is the natural logarithm, N is the number of epochs, $\mathbf{C}$ is the data covariance matrix, and $\hat{\mathbf{v}}$ are the postfit

residuals from some linear (or nonlinear) model applied to the original time series using weighted least squares with the same covariance matrix **C**. The model typically consists of an intercept, a linear trend (velocity), and sinusoidal terms for an annual (and possibly semiannual) signal. The model may also contain terms for offsets (either artificial or coseismic) and, in the event of a large coseismic event, some form of decay term to describe postseismic motion [e.g., *Nikolaidis*, 2002]. The covariance matrix **C** can represent many forms of Gaussian stochastic noise such as white, power law, first-order Gauss Markov, autoregressive, moving average, band pass together with a multitude of combinations of the above. In this paper we assume that **C** is the combination of two noise sources, a white noise component and a power law noise component such that

$$\mathbf{C} = a_w^2 \mathbf{I} + b_\kappa^2 \mathbf{J}_\kappa, \tag{4}$$

where a_w and b_κ are the white and power law noise amplitudes, respectively, **I** is the $N \times N$ identity matrix, and $\mathbf{J}_\kappa$ is the power law noise covariance matrix with spectral index κ. The maximum likelihood problem is typically solved using the downhill simplex method [see *Press et al.*, 1992].

[20] The time series may, of course, contain more than two noise sources, and some, or all of them, may not be power law noise. The theme of this paper is a reconnaissance of the noise present in a lot of stations as seen by several processing centers and as such is assisted by limiting the number and type of noise models to a minimum. A thorough examination of different models and their combinations will be done in the future using a few representative stations.

4.1. Power Law Noise With Integer Spectral Indices and White Noise

[21] In previous error analysis studies of GPS time series [*Zhang et al.*, 1997; *Mao et al.*, 1999; *Calais*, 1999] involving MLE, the power law noise was restricted to two special forms, random walk ($\kappa = -2$) and flicker ($\kappa = -1$) for which a derivation of the covariance matrix existed. Three noise models were tested, white noise only, white noise plus flicker noise, and white noise plus random walk noise. The preferred model, white noise plus flicker noise, was the model having the largest log likelihood value for most sites. A check on the spectral index was performed by fitting a function to the power spectrum of each component of each time series. *Zhang et al.* [1997] fit just a single power law noise to their spectrum and derived a mean spectral index of -0.4 ± 0.1. *Mao et al.* [1999] fit a power law plus white noise curve to the data. The weighted mean of the estimated spectral index for all three components was -0.89 ± 0.28. However, both Zhang et al. and Mao et al. noted that the power spectral method does not produce particularly accurate estimates of the spectral index, an opinion confirmed by *Beran* [1994] and *Langbein and Johnson* [1997]. The main reason for choosing specific spectral indices was that at the time of the previous studies, no general form for the covariance matrix of power law noise was known. The exact covariance matrix for random walk noise was given by *Langbein and Johnson* [1997], while an approximation for the flicker noise covariance matrix was given by *Zhang et al.* [1997] and derived from an algorithm described by *Gardner* [1978] for generating such noise. There are some advantages to assuming a specific type of noise model for all the time series. First, it is easier to compare the noise characteristics of data sets if a parameter or noise model is held fixed. Second, it is easy to assume that all sites are, to some extent, affected by the same noise sources such as monument motion [*Langbein and Johnson*, 1997], atmospheric loading [*vanDam et al.*, 1994], and reference frame [*Herring*, 2000b] and should therefore have a similar power spectrum. Third, MLE poses a large computational burden, in particular if the time series is long or there are many noise model parameters to solve. This burden can be reduced by keeping the number of models to test to a minimum. If the purpose is to provide more robust uncertainties on the linear model parameters, for instance, the site velocity, then a model such as white noise plus flicker noise might not be exact, but it may be close enough and certainly better than the traditional "null" hypothesis of white noise. For the above reasons and for the ease of comparison with the previous studies we initially chose to investigate the three power law noise models described above.

4.2. Power Law Noise With Any Spectral Index and White Noise

[22] Counter arguments to the above suggest that the spectral index should also be estimated. First, stochastic models can provide clues in the search for the physical phenomena that affects the time series. For example, random walk noise due to monument motion is widely regarded as being present in geodetic time series. However, except for the 50 m baseline at Piñon Flat Observatory [*Johnson and Agnew*, 2000], random walk has not been found in GPS time series, probably due to the shortness of the time series and the dominance of other noises. The dominant noise signal so far is something near to flicker noise, and it is spatially correlated and therefore caused by some other phenomena. The search should be for something that produces flicker like noise. Second, we now have a method for producing the power law covariance matrix for any spectral index. The power law covariance matrix, $\mathbf{J}_\kappa$, is computed by means of fractional differencing/integration [*Hosking*, 1981; *Johnson and Wyatt*, 1994] and is described by *Williams* [2003a]. Third, as computing power continues to increase, what was a computational burden in the past may now not be such a problem. Therefore we have also applied the MLE to estimate the spectral index of the time series. There is, however, still a large computational burden. For example, the longest time series analyzed in this study is site YELL in the SOPAC global solution with 3722 data points. Estimating the noise parameters for the white plus flicker noise model took 4 hours for all three components. Estimating the spectral index along with the noise magnitudes took $4\frac{1}{2}$ days. The MLE algorithm is performed in two stages to speed up the computation. The "inner" stage uses the downhill simplex algorithm to find the noise parameters for a given, fixed, spectral index in the same manner as the fixed models above. The "outer" stage uses the Brent method [*Press et al.*, 1992] to find the spectral index that returns the maximum log likelihood value.

Table 2. Test Results of Spectral Index Analysis Using the MLE Algorithm on Synthetic Time Series

Number of Points	Mean Index	RMS	Number of Simulations
3.5 mm White Noise; 8.5 mm/yr$^{1/4}$ Flicker Noise			
256	−0.70	0.51 ± 0.01	2000
365	−0.73	0.36 ± 0.01	720
500	−0.78	0.31 ± 0.02	100
1000	−0.87	0.20 ± 0.01	300
2000	−0.95	0.13 ± 0.01	44
3000	−1.03	0.10 ± 0.02	9
256[a]	−1.06	0.55 ± 0.03	200
256[b]	−0.82	0.27 ± 0.01	200
0.7 mm White Noise; 8.5 mm/yr$^{1/4}$ Flicker Noise			
256	−1.04	0.18 ± 0.01	200
256[a]	−0.96	0.19 ± 0.01	200
8.5 mm/yr$^{1/4}$ Flicker Noise Only			
256	−1.02	0.16 ± 0.01	100
365	−0.99	0.13 ± 0.01	100
500	−0.97	0.10 ± 0.01	30
1000	−1.01	0.07 ± 0.01	30
2000	−1.02	0.05 ± 0.01	30
4.0 mm White Noise; 9.0 mm/yr$^{1/2}$ Random Walk Noise			
365	−1.56	0.61 ± 0.03	300
500	−1.70	0.49 ± 0.03	100
1000	−1.86	0.31 ± 0.01	300

[a]In this test, no slope or intercept was estimated while calculating the spectral index and noise parameters.
[b]In this test the white noise was not estimated but was fixed at the correct value.

[23] *Langbein and Johnson* [1997] and *Mao et al.* [1999] demonstrated with synthetic data that the MLE technique could recover accurate and precise estimates of the noise magnitudes and their uncertainties. They also tested power spectral analysis of the time series for estimating the spectral index. *Langbein and Johnson* [1997] concluded that while the method could establish that the simulated data contained colored noise, the estimates of the index were biased low and the estimates of the random walk component were not very accurate. *Mao et al.* [1999] found that they could estimate reliable indices from time series of 2 years or longer. However, the indices estimated from the power spectra appeared to be biased even from time series of 15 years in length. The usefulness of estimation using the power spectrum is discussed by *Beran* [1994]. We tested the MLE method on synthetic time series of varying lengths (Table 2). For short time series the mean spectral index is biased low. When there is 3.5 mm of white noise and 8.5 mm/yr$^{1/4}$ of flicker noise, a ratio typical of the global GPS time series studied in this paper, then the bias is negligible for series longer than around 2000 to 3000 points. For random walk noise with a similar ratio, the length needed is even longer. The rate of convergence of the RMS of the estimated indices is approximately $n^{-1/2}$ as predicted by *Beran* [1994]. Three factors contribute to the index bias and size of the RMS: the ratio of the two noise amplitudes (b_κ/a), the length of the series, and a trade-off between the trend in the time series due to tectonic motion and the trend due to the noise.

[24] The ratio of the two noise amplitudes is a proxy for the crossover frequency, i.e., the frequency at which the two processes have equal power. If a time series is assumed to contain two noise sources, then the overall length of the series must be at least longer than the crossover period. Typically, the length of the series must be sufficient for the power law noise to be "visible" over the white noise. For flicker noise plus white noise a ratio of $b_{-1}/a \approx 11$ leads to a crossover frequency equal to the daily sampling frequency, and therefore the flicker noise dominates. Ratios lower than this indicate that the crossover frequency is within or lower than the range of frequencies covered by the time series. The simulated series with no white noise or 0.7 mm white noise and 8.5 mm/yr$^{1/4}$ of flicker noise show little or no bias at only 256 points and a significantly reduced RMS. Unlike the previous studies this MLE algorithm tested for single noise models, i.e., white noise only or power law noise only which reduced or even eliminated the failure of the algorithm to converge. When the number of points in the series was small and/or the noise ratio high, then the algorithm would often prefer a power law only model. The series was of insufficient length to detect the presence of two noise models but still acknowledged the presence of correlated noise. A single power law noise model would be biased low. In one experiment the white noise was fixed to its correct amplitude and not estimated. The bias was lower than when both noise amplitudes were estimated and the RMS was reduced.

[25] Removal of a trend from the data removes significant amounts of power from the spectral estimates at the lowest frequencies [*Langbein and Johnson*, 1997; *Johnson and Agnew*, 2000]. A trend is estimated in the real data because it is assumed the data represent tectonic motion. However, power law noise in a series will also possess a trend, and there is no way to split the trend into its two components. By fitting a trend, all of it has been attributed to tectonics causing a low bias in the estimated spectral index, that is, closer to zero. If no trend is estimated from the synthetic series, which have no trend, we see that there is no bias even for series with only 256 data points. Therefore the spectral indices derived from the shorter CGPS time series in this study should be treated with caution noting that they are likely biased low.

5. Results

5.1. Integer Spectral Index Analysis

[26] In the previous studies, *Zhang et al.* [1997] and *Mao et al.* [1999] produced tables of log likelihood for each site, for each component, and for each of the three models. With 954 sites in this study we summarize the results for each solution in Table 3. The north, east, and vertical components are treated separately, giving 2862 log likelihood comparisons. For all solutions, white noise plus flicker noise or white noise plus random walk noise is generally preferred to a white noise only model. At the sites where white noise only is preferred, the length of the time series is short, typically under 2 years of data. The shortness of the series is probably such that the time-correlated component cannot be determined when forced to be an integer spectral index. In section 5.2, when the spectral index is estimated, the most likely noise model for these sites is a power law only noise model with low spectral index and no white noise. While time-correlated noise is likely to exist at these sites, the length is preventing a significant determination of the

Table 3. Summary of the Log Likelihood Tests for the Integer Spectral Index Analysis[a]

Solution	Models		
	wn + fn, %	wn + rw, %	wn, %
SOPAC global	96.6	3.4	0.0
JPL global	97.4	2.6	0.0
SOPAC SCIGN	76.0	21.8	2.2
JPL SCIGN	59.8	33.3	6.9
USGS SCIGN	89.9	9.2	0.9
PANGA PANGA	88.3	10.5	1.2
SOPAC PANGA	71.1	28.9	0.0
SOPAC BARGEN	75.2	24.8	0.0
REGAL REGAL	96.8	3.2	0.0

[a]Models are white noise plus flicker noise (wn + fn), white noise plus random walk noise (wn + rw) and white noise only (wn). Columns represent the percentage of time series for which the log likelihood value for a specific model is the highest. The higher the log likelihood, the more significant and likely the model is as a candidate for the noise in the time series.

properties. However, the presence of colored noise in the GPS time series is confirmed. White noise plus flicker noise is clearly the dominant noise model, although there are more sites in the regional solutions where white noise plus random walk noise is preferred.

[27] The maximum log likelihood values confirm that of the three models, white noise plus flicker noise is the preferred model, as suggested by *Zhang et al.* [1997], *Mao et al.* [1999], and *Calais* [1999]. Therefore only the amplitudes from the white noise plus flicker noise analysis are presented here. A summary of the noise magnitudes for each solution is provided in Table 4 and, for those sites in the SCIGN array that are common to five different solutions, in Figure 4.

[28] For the two global solutions we find that as expected, the horizontal components are less noisy for white and flicker noise magnitudes than the vertical components by a factor of 2–3. The east components, also as expected, are somewhat noisier than the north components because of no (SOPAC) or incomplete (JPL) integer-cycle phase ambiguity resolution in the global solutions. The white noise amplitudes are about 2 times larger in the JPL global solutions compared to the SOPAC global solutions, in all three components, while the flicker noise amplitudes are only marginally larger. The white noise amplitude differences are probably due to processing strategies (what these may be are beyond the scope of this paper), while the comparable flicker noise amplitudes may reflect a common physical basis, such as seasonal atmospheric mass distributions [e.g., *Dong et al.*,

Table 4. Mean, Weighted Mean, and Median of the White Noise and Flicker Noise Amplitude Estimate for the North, East, and Vertical Components of the Site Time Series for Each Solution[a]

Solution	White Noise, mm			Flicker Noise, mm/yr$^{1/4}$		
	North	East	Vertical	North	East	Vertical
SOPAC global						
Mean	1.5 ± 0.6	2.3 ± 1.0	3.9 ± 1.9	5.3 ± 2.2	7.6 ± 3.0	20.2 ± 5.5
Weighted mean	1.4	2.1	3.9	4.9	6.8	20.1
Median	1.3 ± 0.4	2.0 ± 0.5	3.3 ± 0.9	4.3 ± 1.8	6.6 ± 1.8	18.7 ± 3.4
JPL global						
Mean	3.0 ± 0.7	4.6 ± 1.9	7.7 ± 2.6	7.7 ± 2.1	10.6 ± 4.2	23.1 ± 7.8
Weighted mean	2.9	4.1	7.3	7.6	9.6	22.0
Median	2.8 ± 0.6	4.1 ± 1.1	7.0 ± 2.0	7.3 ± 2.3	9.6 ±3.0	21.5 ± 6.6
SOPAC SCIGN						
Mean	0.8 ± 0.2	0.9 ± 0.4	3.0 ± 0.5	2.2 ± 1.6	2.3 ± 1.5	7.0 ± 5.0
Weighted mean	0.7	0.8	3.0	2.2	2.1	7.2
Median	0.7 ± 0.2	0.8 ± 0.3	3.0 ± 0.6	1.9 ± 1.1	1.9 ± 1.3	5.8 ± 3.7
JPL SCIGN						
Mean	0.9 ± 0.3	1.1 ± 0.5	3.6 ± 0.9	2.0 ± 0.8	2.1 ± 1.0	7.0 ± 3.2
Weighted mean	0.8	0.9	3.3	1.8	1.7	6.5
Median	0.9 ± 0.4	1.0 ± 0.5	3.6 ± 1.5	2.0 ± 1.3	2.0 ± 1.4	5.7 ± 4.3
USGS SCIGN						
Mean	1.4 ± 0.4	1.8 ± 0.5	4.1 ± 1.0	3.1 ± 1.7	3.6 ± 1.5	9.2 ± 3.7
Weighted mean	1.1	1.6	3.7	2.5	3.4	8.4
Median	1.2 ± 0.7	1.6 ± 0.8	4.0 ± 1.4	2.9 ± 1.9	3.3 ± 1.5	8.5 ± 3.5
PANGA PANGA						
Mean	1.7 ± 0.8	2.3 ± 1.1	5.0 ± 1.9	3.9 ± 2.0	4.4 ± 2.0	12.5 ± 4.9
Weighted mean	1.4	1.7	4.6	3.3	3.6	11.0
Median	1.4 ± 0.9	1.9 ± 1.4	4.6 ± 2.5	3.8 ± 2.4	3.8 ± 2.5	11.4 ± 6.6
SOPAC PANGA						
Mean	0.6 ± 0.2	0.8 ± 0.4	2.4 ± 0.7	2.7 ± 1.1	2.8 ± 1.0	8.6 ± 4.0
Weighted mean	0.6	0.7	2.4	2.4	2.4	8.5
Median	0.6 ± 0.2	0.7 ± 0.3	2.2 ± 0.6	2.5 ± 1.6	2.5 ± 0.9	7.7 ± 2.5
SOPAC BARGEN						
Mean	0.5 ± 0.1	0.7 ± 0.1	2.3 ± 0.6	1.3 ± 0.4	1.3 ± 0.6	5.5 ± 2.2
Weighted mean	0.5	0.6	2.2	1.2	1.2	4.9
Median	0.5 ± 0.1	0.7 ± 0.2	2.2 ± 0.5	1.2 ± 0.4	1.2 ± 0.7	5.4 ± 3.1
REGAL REGAL						
Mean	2.0 ± 0.7	2.2 ± 0.6	4.2 ± 1.1	5.0 ± 1.6	5.0 ± 1.3	10.9 ± 5.5
Weighted mean	1.7	1.9	3.4	4.5	4.6	8.8
Median	1.8 ± 1.2	2.0 ± 0.9	4.1 ± 1.0	4.7 ± 2.2	4.8 ± 2.4	8.7 ± 6.0

[a]The range indicated by the plus/minus is the standard deviation for the mean and the interquartile range (IQR) for the median.

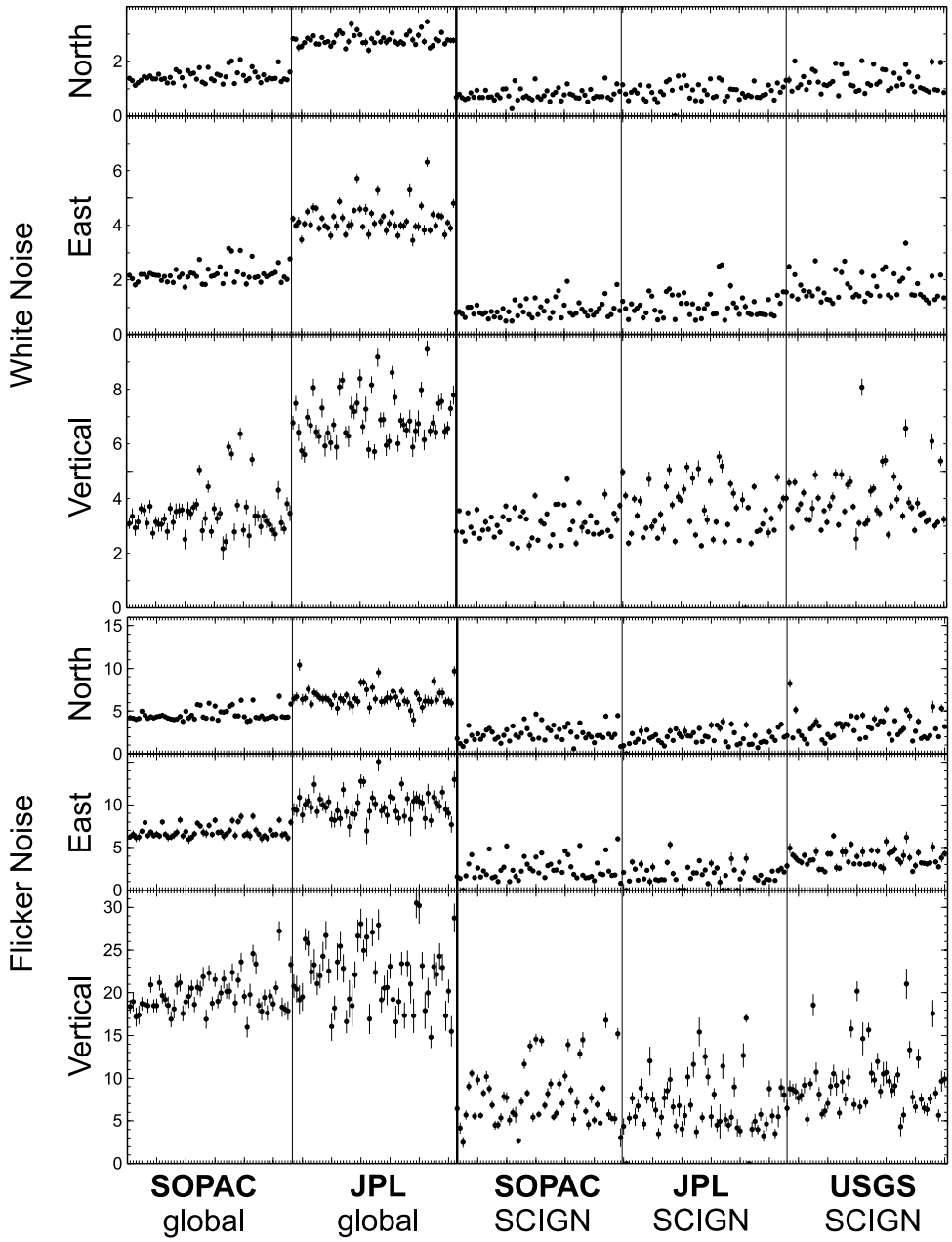

Figure 4. Comparison of white noise and flicker noise amplitudes in the north, east, and vertical components for those sites in the SCIGN array that are in five different solutions. Error bars are 1σ formal errors.

2002] atmospheric noise [*Williams et al.*, 1998], or second-order ionospheric effects [*Kedar et al.*, 2003].

[29] For the SOPAC and JPL regional solutions the results are strikingly similar in both white noise and flicker noise magnitudes and in all three directions. In this case, the north and east noise amplitudes are nearly the same, reflecting essentially complete and successful phase ambiguity resolution. The vertical magnitudes are about 3 times larger than the horizontal magnitudes. Removing the common mode signature (though using different approaches) significantly reduces (by a factor of 2–3) the amplitudes of both the white noise and flicker noise components, supporting our explanation that a significant amount of the flicker noise is due to a common physical basis with large spatial extent. The remaining flicker noise is probably due to regional-scale processes such as atmospheric effects, not to monument motion which is thought to follow a random walk process. Both noise components are therefore spatially correlated to some extent. This can also be seen in the power spectrum of the common mode signal from the SOPAC SCIGN (regional) solution (Figure 5). The common mode signal has flicker noise magnitude of 5.6, 7.0, and 21.6 in north, east, and vertical, respectively, and white noise magnitudes of 1.9, 2.7, and 4.3 (NEU), which are very similar to the average noise magnitudes in the SOPAC global solution.

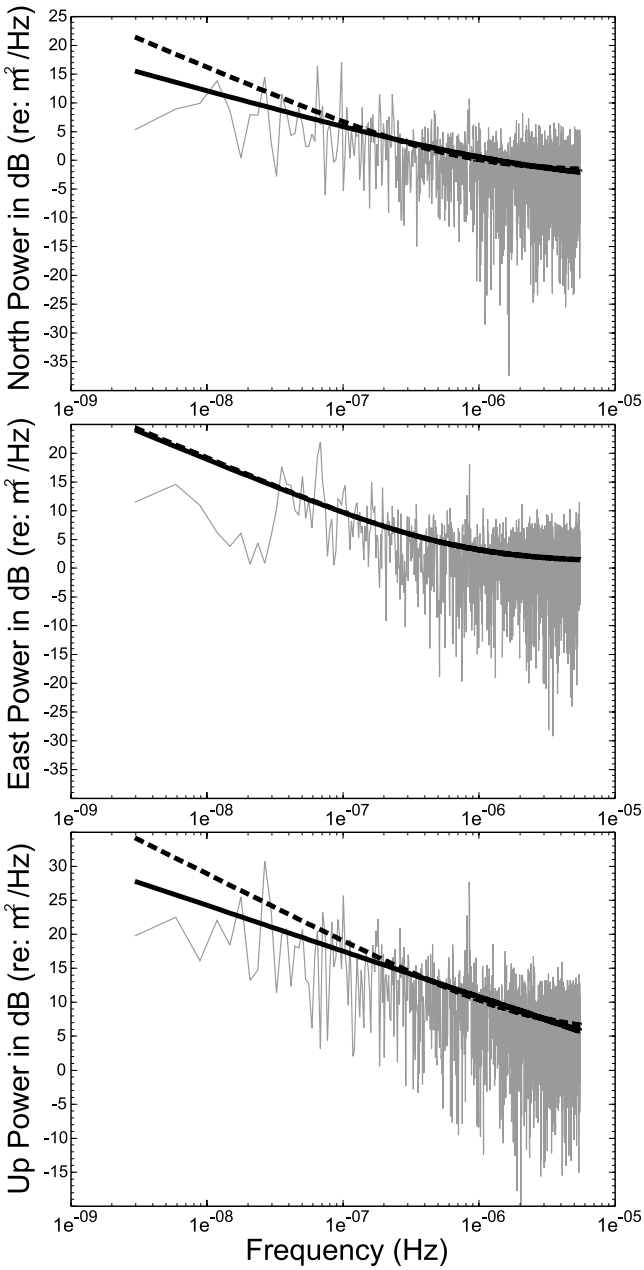

Figure 5. Power spectrum in the north, east, and vertical components of the common mode noise in the SOPAC regional SCIGN solution. Solid line is the fitted spectra of white noise and flicker noise based on the average amplitudes from the SOPAC global solution. Dashed line is the fitted spectra of white noise and flicker noise estimated using the MLE algorithm on the common mode time series. Note also the prominent peak at around a period of 13.6 days. This is also seen in the JPL global time series. An explanation of this is provided by *Penna and Stewart* [2003].

[30] The USGS solution is about 50% worse than the SOPAC or JPL (regional) solutions in both noise processes and in all coordinate components. This may be accounted for by the fact that the USGS solution is based on a rapid analysis of the data before the more accurate IGS final orbits are available since both SOPAC and USGS use the GAMIT/GLOBK software, although with different processing strategies. The significantly lower noise magnitudes for the SOPAC PANGA analysis compared to the PANGA PANGA analysis is most likely due to not resolving integer-cycle phase ambiguities in the latter analysis after point positioning. In addition, the PANGA analysis group use sites outside of the array and fewer sites to remove common mode signals. The same factors may explain the larger noise magnitudes in the REGAL REGAL solution. The SOPAC SCIGN solutions show slightly lower flicker noise amplitudes and slightly higher white noise amplitudes than the SOPAC PANGA solutions. The lower flicker noise in the SOPAC SCIGN solutions may be due to more variable meteorological conditions in the Pacific Northwest compared to southern California, while the higher white noise amplitudes may be due to the longer SCIGN time series.

[31] The SOPAC BARGEN solution provides the lowest noise amplitudes for both noise processes and all components. There are several reasons for this. BARGEN is the most homogeneous network tested in terms of monumentation (Wyatt-designed deep drill braced monuments, in rock) and environment (desert conditions). It is noteworthy that the white noise plus flicker noise model is still preferred over the white noise plus random walk model, indicating that monument noise is still not the limiting factor. On the other hand, the BARGEN sites are generally younger than the SCIGN sites, explaining the reason for the lower white noise amplitudes in the SOPAC BARGEN solutions.

[32] *Mao et al.* [1999] found a latitude dependence for white noise in the vertical component. With around an order of magnitude more stations in this study we can investigate latitude dependence in the global solutions. The white and flicker noise amplitudes as a function of site latitude is plotted in Figure 6 for the JPL and SOPAC global solutions. Also plotted is an arbitrarily derived function to highlight any midlatitude dependence and a hemisphere bias. The function takes the form

$$\sigma = \begin{cases} a + be^{-c\lambda^2} & \lambda > 0 \\ a + d\left\{e^{-c\lambda^2} - 1\right\} + b & \text{otherwise,} \end{cases} \quad (5)$$

where σ is the noise amplitude, λ is the site latitude, and a, b, c, d are the estimated parameters. Using the standard F test, we found that for the white noise magnitude in all three components and for both solutions we could reject the null hypothesis that the noise was equal at all latitudes. In the case of the flicker noise we could only reject the null hypothesis for the east component in both solutions. However, the fit to the data does suggest that there is a latitude dependence in the north and vertical components. In all cases the fit to equation (5) showed a significant positive bias for Southern Hemisphere sites i.e., sites in the Southern Hemisphere are noisier than sites in the Northern Hemisphere.

[33] It seems likely that as the number of sites available for the global reference frame increases the noise in the time series should decrease. To see whether this is indeed the case, we took some of the longest sites and analyzed 2 years worth of data from the series, stepping every year; that is, we analyzed 1991–1993, 1992–1994, 1993–1995, etc. We used those sites with more than 3000 epochs in

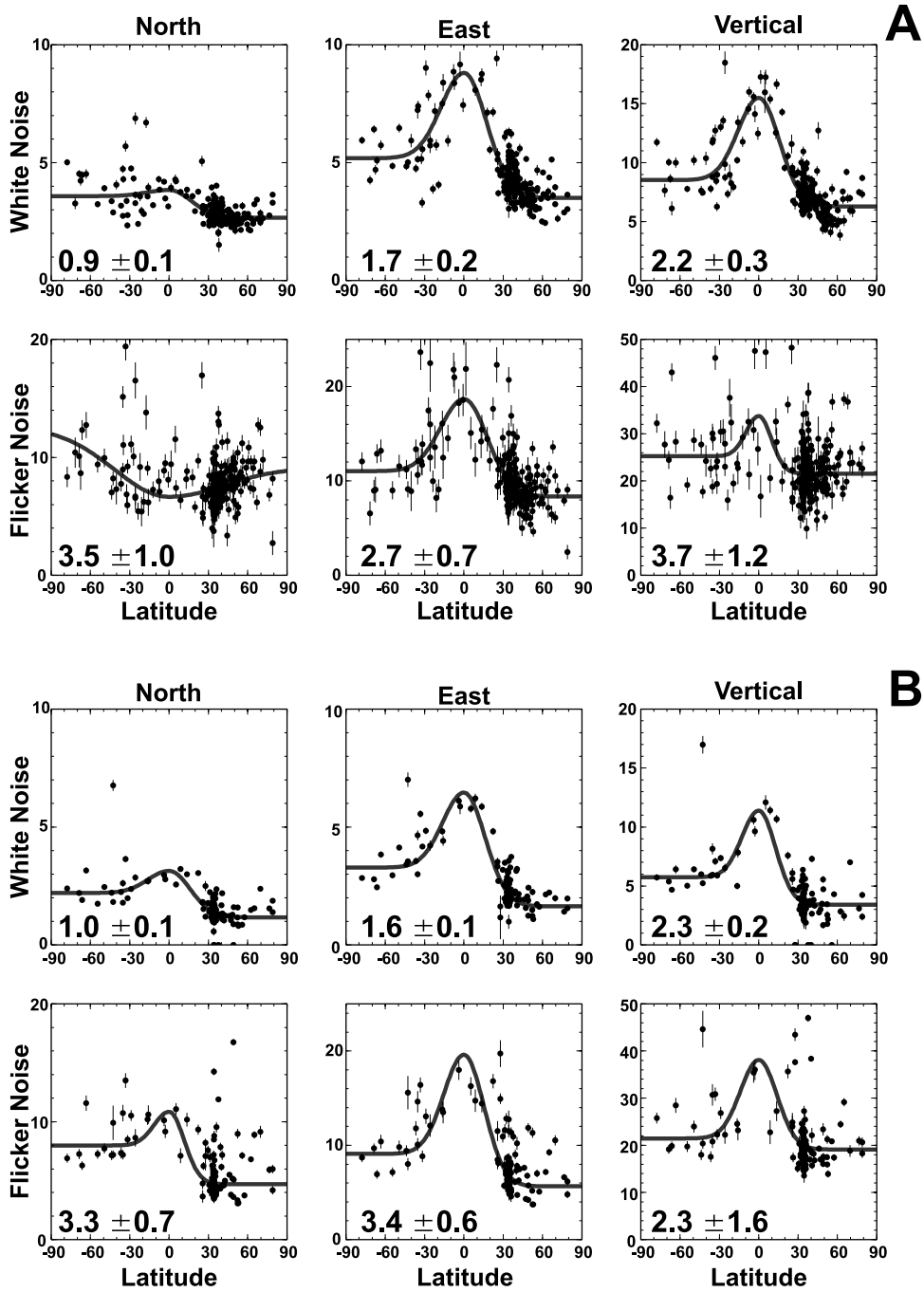

Figure 6. White noise and flicker noise amplitudes as a function of latitude for the two global GPS solutions: (a) the JPL (SCIGN_1.0.0) global solution and (b) the SOPAC global solution. Note the different scales on the *y* axis. The hemisphere bias and its formal error are plotted on each panel; positive indicates larger amplitudes in the Southern Hemisphere. Uncertainties are 1σ formal errors.

their series. We could therefore look at three solutions, SOPAC global (17 sites), JPL global (12 sites), and SOPAC SCIGN (5 sites). The weighted mean for each time span is plotted for the three solutions in Figure 7. A weighted least squares fit to the data of a slope and intercept is also plotted in Figure 7, and the values are listed in Table 5. In all cases, apart from the vertical component of white noise in the JPL global solution, there is a significant decrease in noise with time. This result reflects the improvement in the global reference frame and the resulting improvements in analysis products (e.g., satellite orbits, Earth orientation parameters).

5.2. Power Law Noise With Estimated Spectral Index and White Noise

[34] The spectral indexes for all three components of the 954 time series were estimated (Figure 8). The spectral indices range from −3.0 (vertical component of GOL2 in the JPL SCIGN solution) to 1.0 (east component of ERLA in the PANGA PANGA solution, 597 points) with a mean

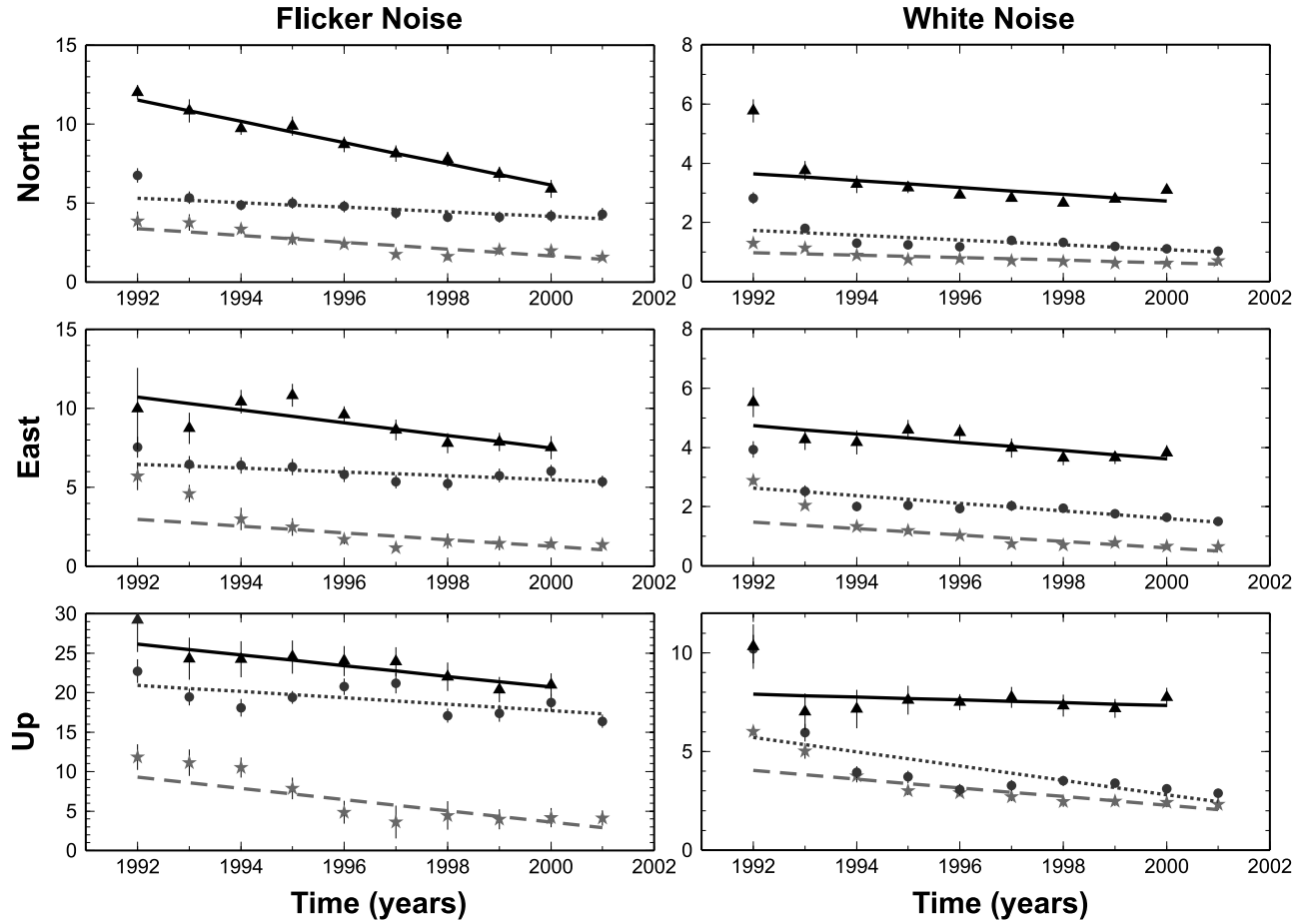

Figure 7. White noise and flicker noise amplitudes in the north, east, and vertical components as a function of the median time of the analysis period. Triangles indicate the results from the JPL SCIGN_1.0.0 global solution. Circles are from the SOPAC global solution. Stars are from the SOPAC SCIGN solution. Uncertainties are 1σ formal errors.

index of −0.92 and standard deviation of 0.43. By individual components the means and standard deviations are −1.0 ± 0.5 (north), −0.9 ± 0.4 (east), and −0.8 ± 0.4 (vertical). The two global solutions show a mean and standard deviation that is consistent with the values seen for the simulated time series containing white noise plus flicker noise. Our larger database of values from longer time series confirm the previous conclusions of *Mao et al.* [1999] and *Zhang et al.* [1997] that the noise processes in GPS time series can be adequately described by a white noise plus flicker noise model. The larger spread of estimates for the regional solutions suggests a combination of noise sources

Table 5. Estimated Slope and Intercept Parameters for the Change in Amplitudes of White Noise and Flicker Noise as a Function of Time[a]

	White Noise		Flicker Noise	
	Intercept, mm	Slope, mm/yr	Intercept, mm/yr$^{1/4}$	Slope, mm/yr$^{5/4}$
		SOPAC Global		
North	1.73 ± 0.08	−0.08 ± 0.01	5.32 ± 0.29	−0.15 ± 0.05
East	2.63 ± 0.12	−0.13 ± 0.02	6.46 ± 0.36	−0.12 ± 0.06
Up	5.71 ± 0.27	−0.36 ± 0.05	20.95 ± 0.86	−0.40 ± 0.14
		JPL Global		
North	3.65 ± 0.17	−0.12 ± 0.03	11.53 ± 0.48	−0.67 ± 0.09
East	4.74 ± 0.25	−0.14 ± 0.04	10.72 ± 0.63	−0.40 ± 0.11
Up	7.90 ± 0.52	−0.07 ± 0.09	26.15 ± 1.60	−0.68 ± 0.30
		SOPAC SCIGN		
North	0.98 ± 0.07	−0.04 ± 0.01	3.38 ± 0.27	−0.22 ± 0.04
East	1.48 ± 0.13	−0.11 ± 0.02	2.97 ± 0.38	−0.21 ± 0.06
Up	4.03 ± 0.28	−0.22 ± 0.04	9.31 ± 1.31	−0.71 ± 0.21

[a]The reference used for the intercept is 1992. Errors are 1σ formal errors.

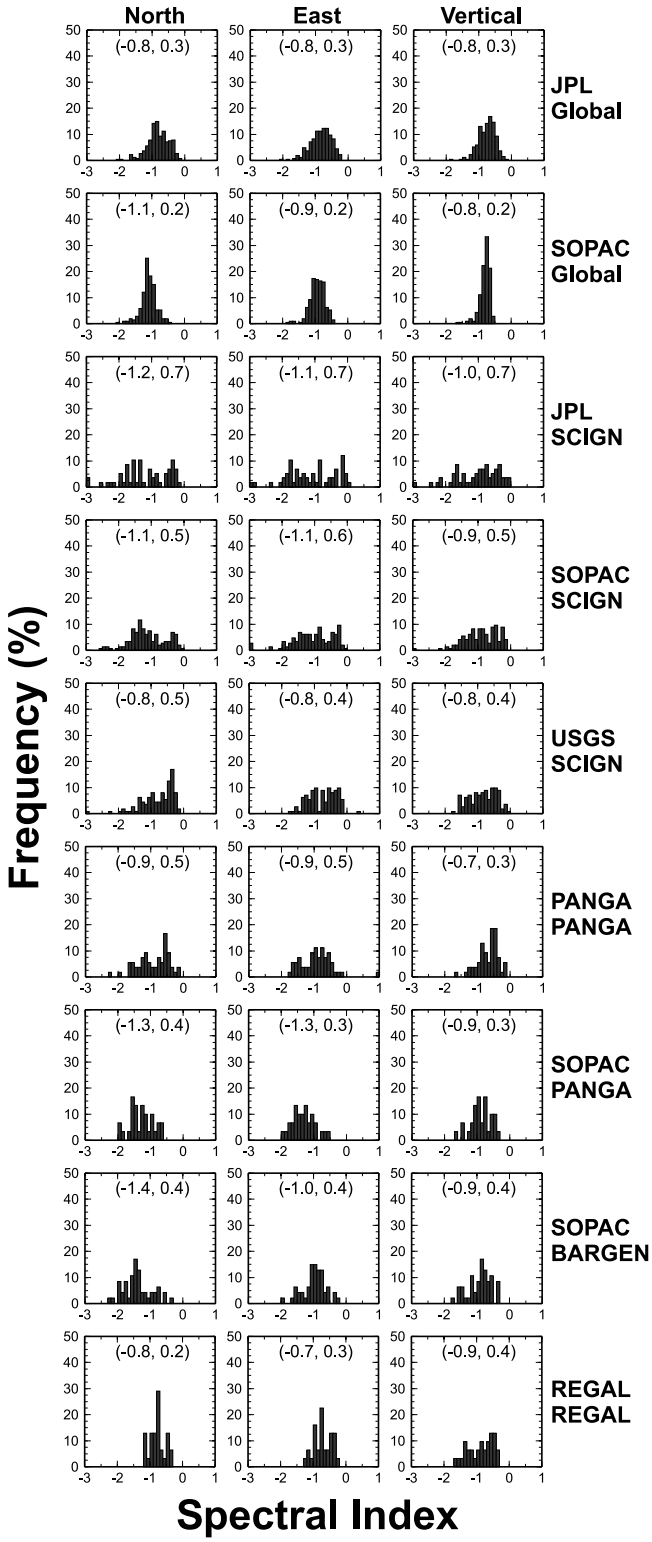

Figure 8. Histograms of the estimated spectral index for the north, east, and vertical components at sites in the different GPS solutions. Values inside the parentheses indicate the mean and standard deviation of the spectral estimates.

instead of perhaps a single dominant signal in the global solutions. These noise sources may be due to a combination of differences in atmospheric effects from region to region and local site effects such as type and variety of geodetic monuments (discussed further below), as well as other local conditions. For example, in southern California, *Bawden et al.* [2001] and *Watson et al.* [2001] found widespread groundwater and oil pumping that contaminated the tectonic signal measured at certain GPS stations. An excellent correlation can be found between sites whose time series are expected to be contaminated (see also http://quake.wr.usgs.gov/research/deformation/modeling/socal/la.html) and those in this study with spectral indices lower than around -1.5. For example, FVPK has spectral indices of -2.7, -2.2, -0.9 for north, east, and vertical, respectively. The uncharacteristically large spectral indices are due in this case to unmodeled nontectonic deformation at these sites.

5.3. Spatial Correlation

[35] The reduction in time-correlated noise from global solutions to regional solutions, which have had common mode noise removed, suggests that some of the noise is spatially correlated. We can examine this by examining the correlation between time series of sites in a solution as a function of the station separation (Figures 9 and 10). The site-to-site correlations are calculated from the residuals, thereby removing the influence that a trend and annually repeating signal would have on the estimated value.

[36] Traditionally, the significance of any correlations is tested with the implicit assumption that the two series are white. In this case, if the two series are uncorrelated and the number of common points is sufficiently large ($N > 500$ say), then the estimated correlation coefficient is distributed normally with a zero mean and a standard deviation of $N^{-1/2}$ [*Press et al.*, 1992]. Other methods have been proposed to account for non-Gaussian probability distributions; however, these may still be inappropriate for time-correlated noise. The danger of spurious correlations in economic time series was discussed by *Granger and Newbold* [1977]. They performed simulations on several time-correlated noise models and showed that high correlations that would be considered significant from the standard tests were achieved from two uncorrelated series. We performed similar simulations to investigate the significance of the spatial correlations seen here. Pairs of time series with noise similar to what we would expect for the global sites in the horizontal (8.5 mm/yr$^{1/4}$ flicker, 3.5 mm white) and vertical (21 mm/yr$^{1/4}$ flicker, 6 mm white) were simulated. Time series of length 32, 64, 128, 256, 512, 1024, and 2048 were used. In this case, a decrease in standard deviation of the estimated correlation is seen with length, but it is slower than the $N^{-1/2}$ for white noise. Further, the standard deviation tended to a steady value of just below 0.1 for large N. With this in mind, we can be confident of the significance of the correlations seen in Figures 9 and 10.

[37] In the two global solutions (Figure 9) a gradual decrease in correlation is seen from about 0.8 at around 0.1° (10 km) to a correlation of 0.5 at around 10° (1000 km). The correlation drops sharply to zero at around 40°. In the JPL global solution the correlations between the PIN1 and PIN2 sites, which are 50 m apart, are 0.79, 0.78, and 0.72 (753 common epochs) in north, east, and vertical compo-

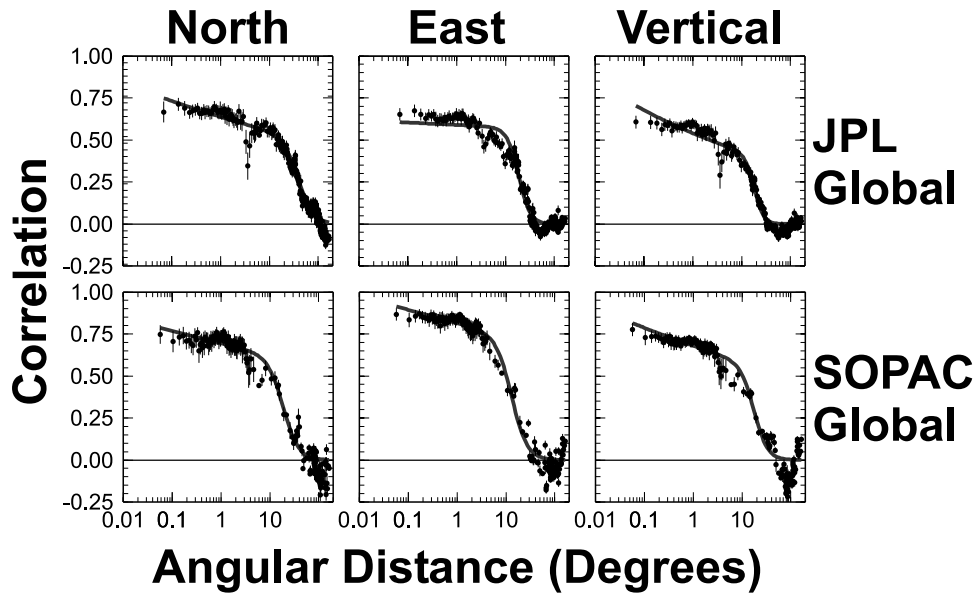

Figure 9. Correlation of time series for north, east, and vertical components for the two global solutions as a function of station separation in degrees. Individual points are the weighted mean (and its 3σ error) of 100 individual correlation estimates. Weighting is based on the number of points in the series used to calculate the correlation. Solid line is an arbitrary fit to the data that assumes the correlation tends to zero at large distances and incorporates a break in slope at an unspecified angle.

nents, respectively. In the SOPAC global solution the correlations for PIN1-PIN2 are 0.88, 0.88, and 0.85 (2691 common epochs). Note that the closeness of the sites is not taken into account in either the JPL or SOPAC global solutions.

[38] In the regional solutions the picture is less clear (Figure 10). In the JPL SCIGN solution the correlations are virtually zero at all station separations; that is, there is no common mode signal remaining in the time series. In the SOPAC and USGS SCIGN solutions, correlations are still evident between sites, although they are rarely above 0.5 and decrease quickly to zero correlation for larger site separations. In both PANGA solutions a relatively low correlation is seen across all the angular distances. The PANGA array is larger in extent and has a larger station separation than the SCIGN array so the correlations at small angular distances are not seen. There is a small positive correlation remaining between sites less than 2° apart in the SOPAC BARGEN solution. In the REGAL solution the correlations are larger and are more on par with the correlations seen in the global solutions. However, the decrease in correlation is faster reaching zero correlation at around 8° and continuing to decrease into a negative correlation up to −0.25. The REGAL vertical component has lower overall correlation values but a similar pattern to the horizontal.

[39] The reduction in correlation from the global solutions to the regional solutions is a clear indicator that the common mode noise has, to some extent, been removed in the regional solutions. However, the different degrees to which the common mode noise has been removed can either be attributed to the different methods used to filter out the common mode and/or the number of sites used in the filter. The USGS and JPL SCIGN SCIGN solutions estimate a daily seven-parameter Helmert transformation to a reference frame defined by the positions and velocities of a set of sites. In the USGS solution, 37 sites are used, whereas all the available sites are used in the JPL solution. The SOPAC SCIGN, PANGA, and BARGEN solutions and the PANGA PANGA solutions use the *Wdowinski et al.* [1997] method, which is equivalent to a daily three-parameter (translations only) Helmert transformation in a topocentric (NEU) coordinate system. The PANGA PANGA solution used six sites and the SOPAC SCIGN solution used eight sites. If the difference in reduction was due to the method used, then the USGS solution would be expected to have less spatial correlation and smaller noise amplitudes than the SOPAC SCIGN solution. The SOPAC solution, uses only eight sites to form the common mode signal, yet the noise in the series is comparable to that of the JPL solution. It does, however, suffer from a greater correlation between sites. It seems likely that the number of sites used to remove the common mode noise is the main contributing factor. A preliminary look at the ''production'' time series from SOPAC (at http://sopac.ucsd.edu) and the SOPAC PANGA and SOPAC BARGEN solutions which differ from the *Nikolaidis* [2002] series primarily in the use of a greater number of sites to form the common mode signal appears to show a noise reduction compared to the SOPAC SCIGN solution used here. That the PANGA PANGA and REGAL REGAL solutions have larger noise amplitudes than the SCIGN solutions is related partly to the larger intersite distances and areal extent as well as to other differences described earlier. Since the common mode noise is assumed to be the same over the entire region, the estimated signal is probably representative of the noise near to the center of mass of the reference frame sites. Sites farther away from the center of mass are more likely to suffer from larger noise amplitudes. In arrays such as the SCIGN the common mode noise could be calculated on a subregion basis or possibly even on a site

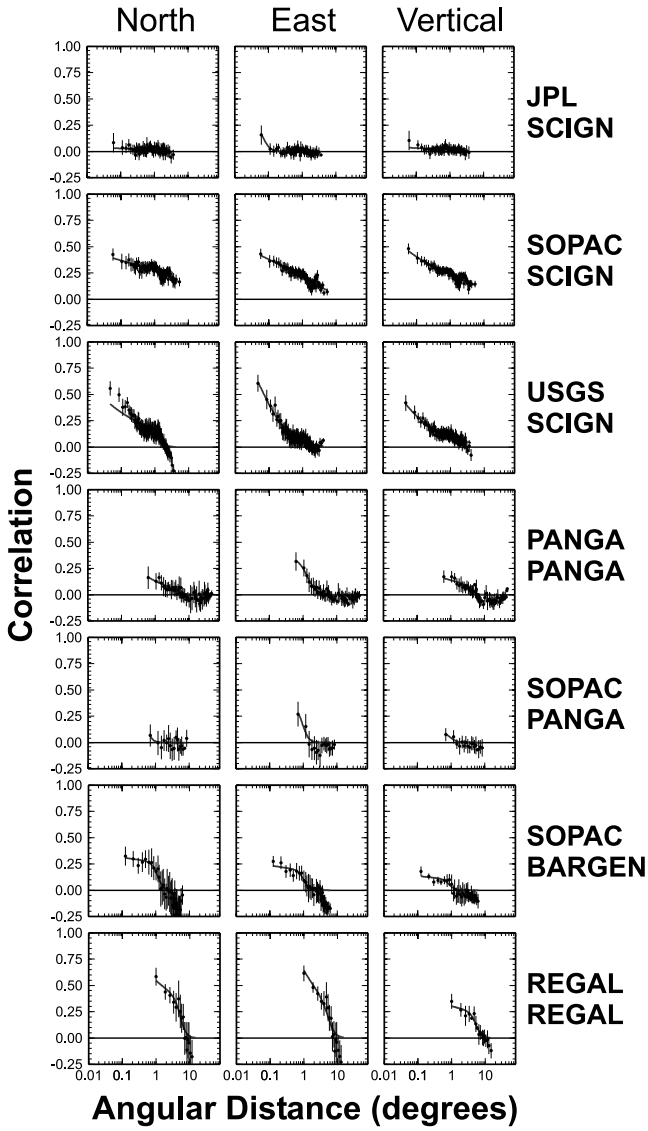

Figure 10. Correlation of time series for north, east, and vertical components for the regional solutions as a function of station separation in degrees. Individual points are the weighted mean (and its 3σ error) of n individual correlation estimates. Weighting is based on the number of points in the series used to calculate the correlation. Solid line is an arbitrary fit to the data that assumes the correlation tends to zero at large distances and incorporates a break in slope at an unspecified angle, and n is 100 for JPL SCIGN_2.0.0 and SOPAC SCIGN, 50 for USGS SCIGN, and 25 for the rest.

by site basis using the observed correlation statistics and kriging [*Journel and Huijbregts*, 1978].

5.4. Monuments

[40] An initial motivation behind this work was to assess the impact of different monuments on the noise in the continuous GPS time series. To achieve this, many time series from sites with different monument types are required. Although the global GPS network has (unfortunately) a large mix of monuments and siting approaches, we have shown that the global solutions are dominated by spatially correlated and latitude-dependent flicker noise. Monument noise in geodetic data sets is perceived to be a random walk process [*Langbein and Johnson*, 1997; *Johnson and Agnew*, 2000]. If random walk monument noise is present in such series at around the 0.4 mm/yr$^{1/2}$, then the series would have to be over 30 years long before it is easily detected. The only likely candidates for assessing monument stability are therefore the regional networks where most of the common mode noise has been eliminated. The only regional network that has sufficient sites with sufficient variation in monument type is the SCIGN array.

[41] A second problem associated with this study is the definition of noise levels. For white noise it is simple, just the magnitude of the noise, i.e., the RMS. For flicker noise (or random walk noise) plus white noise the power law noise component will over time be the dominating influence. However, for the regional solutions we see a range of spectral indices. How then are noise levels conveniently defined? The ratio of power law noise to white noise was used by *Zhang et al.* [1997] as an indicator. The lower the ratio the better the site was assumed to be. However, this does not take into account the overall magnitudes of the noise components. Two sites could have the same ratio, but one site may have noise amplitudes twice as big as another site. In this study we use two parameters, the random walk noise amplitude (b_{-2}) from the white noise plus random walk solutions and the length of time required for the rate uncertainty to reach a specific level (in this case 1 mm/yr) given the parameters derived in section 4.2. The first parameter is used assuming that the remaining noise in the regional time series is random walk noise from monument motion. The second parameter does not assume the type of power law noise present but at least gives us a meaningful figure that is often asked of GPS time series.

[42] We chose to study the SOPAC SCIGN solution since this had the longest history, the largest number of sites and the most diverse types of monuments. Out of the 147 sites we identified eight broad categories of monument type based on descriptions in the site log files, site photographs, and communication with relevant agencies. These monument types include roof/chimney, concrete pier, concrete slab, metal tripod, Wyatt-designed deep drilled braced [*Wyatt et al.*, 1989; *Bock et al.*, 1997], steel tower, rock pin, and oil drilling platform. Note that most of the monument diversity came from the early pre-SCIGN period, starting in 1991, thus providing some of the longest continuous GPS time series available today. The median values for b_{-2} and $T_{1\mathrm{mm/yr}}$ for each component based on monument type are given in Table 6. The monument types in Table 6 have been ranked in increasing order of noise level. The ranking was performed by summing the individual ranks from each component and each parameter and then ranking the sums. In all three components the deep drilled braced monument appears to be the most stable in the sense that it contains the least noise. The significance of these results were tested using a Monte Carlo method and the Wilcoxon rank sum test [*Wilcoxon*, 1945]. In the Monte Carlo test, N samples, where N is the number of sites of a particular monument type, were drawn randomly from the actual set of parameters and the median calculated. This was

Table 6. Median Random Walk Noise Amplitude b_{-2} and Median Time T for the Velocity Uncertainty to Reach 1 mm/yr for Eight Different Monument Types[a]

		North		East		Up	
Monument Type	Number of Monuments	b_{-2}, mm/yr$^{1/2}$	MC Test, %	b_{-2}, mm/yr$^{1/2}$	MC Test, %	b_{-2}, mm/yr$^{1/2}$	MC Test, %
Deep Braced	96	1.6	0.0	1.6	1.4	4.2	0.0
Roof/Chimney	11	2.0	61.0	2.0	72.2	5.2	45.7
Metal Tripod	11	2.2	71.1	2.5	86.2	7.3	91.7
Rock Pin	8	2.7	89.9	2.3	80.0	7.1	86.8
Steel Tower	10	2.4	81.2	3.1	97.1	7.8	95.3
Concrete Slab	4	3.3	93.6	2.0	57.9	10.0	95.5
Concrete Pier	6	4.4	99.9	3.3	97.3	15.2	100.0
Oil Platform	1	13.3	96.6	3.9	85.1	14.0	90.9
		North		East		Up	
Monument Type	Number of Monuments	T, years	MC Test, %	T, years	MC Test, %	T, years	MC Test, %
Deep Braced	96	0.6	0.0	0.6	0.0	1.3	0.0
Roof/Chimney	11	1.0	83.9	0.8	55.5	3.3	97.9
Metal Tripod	11	0.9	69.2	0.9	73.6	2.4	82.0
Rock Pin	8	1.2	90.2	0.8	64.9	3.0	92.1
Steel Tower	10	1.0	87.3	1.4	97.4	3.0	94.2
Concrete Slab	4	1.2	73.2	0.9	65.5	4.4	91.3
Concrete Pier	6	1.6	92.7	1.1	79.3	6.4	99.5
Oil Platform	1	2.1	92.5	1.2	70.0	5.9	87.0

[a]Monuments have been ranked according to these results from most stable (top) to least stable (bottom). Also included are the results of the Monte Carlo test on the probability that the estimated median could be caused by chance.

repeated 1000 times. From this the probability of obtaining a median lower than that estimated for each monument was calculated. The null hypothesis was that all monument types were of equal stability, i.e., should have the same overall median and probability distribution. The deep drill braced monument shows a zero probability that the median value is low by chance except for the east component of the b_{-2} value, which is still only a 1.4% chance (Table 6). For the monument types in the bottom half of the rankings we see very high probabilities (often over 95% chance) that a lower value can be achieved by chance. Therefore the probability of obtaining a higher median by chance for these monument types is low.

[43] The Wilcoxon rank sum [*Wilcoxon*, 1945] is used to test the significance of the null hypothesis that the populations generating two pairs of data (monument types) are identical. The alternative hypothesis is that the medians of the two populations deviate by a nonzero amount. The only monument type to stand out from this test is the deep drill braced monument (Table 7), where 50% of the tests

Table 7. Results of the Wilcoxon Rank Sum Test to Assess the Probability of Monument Types Having a Different Median Noise Level[a]

North	Deep Braced	Roof-Chimney	Metal Tripod	Rock Pin	Steel Tower	Concrete Slab	Concrete Pier	Oil Platform
Deep Braced		1.0	15.1	8.5	32.0	13.0	17.2	25.3
Roof/Chimney	2.5		9.4	84.0	57.3	85.1	80.7	66.7
Metal Tripod	7.4	87.0		35.1	48.1	17.7	88.4	33.3
Rock Pin	4.9	90.4	44.2		57.3	100.0	95.0	66.7
Steel Tower	21.6	77.8	77.8	94.4		53.9	71.3	36.4
Concrete Slab	4.4	41.2	22.6	36.8	36.6		100.0	40.0
Concrete Pier	1.2	21.6	21.6	18.1	21.4	60.9		100.0
Oil Platform	9.3	16.7	16.7	22.2	18.2	40.0	57.1	
East	Deep Braced	Roof-Chimney	Metal Tripod	Rock Pin	Steel Tower	Concrete Slab	Concrete Pier	Oil Platform
Deep Braced		21.4	15.7	8.3	22.2	17.0	45.5	41.1
Roof/Chimney	27.2		45.0	60.0	48.1	41.2	96.1	50.0
Metal Tripod	9.2	71.8		84.0	67.3	94.9	96.1	66.7
Rock Pin	10.7	54.5	100.0		89.7	57.0	66.2	88.9
Steel Tower	14.1	62.2	88.8	76.2		94.5	87.5	90.9
Concrete Slab	37.9	85.1	85.1	93.3	100.0		76.2	80.0
Concrete Pier	16.8	40.4	66.0	75.5	71.3	91.4		100.0
Oil Platform	16.3	33.3	66.7	66.7	36.4	80.0	100.0	
Vertical	Deep Braced	Roof-Chimney	Metal Tripod	Rock Pin	Steel Tower	Concrete Slab	Concrete Pier	Oil Platform
Deep Braced		0.1	0.2	1.5	0.8	1.6	1.3	17.5
Roof/Chimney	21.1		9.4	49.2	67.3	57.1	96.1	33.3
Metal Tripod	0.2	9.4		35.1	43.9	13.9	66.0	33.3
Rock Pin	4.3	35.1	65.7		96.5	57.0	75.5	44.4
Steel Tower	0.2	7.8	83.3	57.3		37.4	100.0	36.4
Concrete Slab	0.9	7.8	48.9	21.4	63.5		100.0	80.0
Concrete Pier	0.0	0.7	3.6	4.3	7.3	47.6		100.0
Oil Platform	12.4	33.3	50.0	44.4	18.2	40.0	100.0	

[a]Values are in percentages; a low percentage indicates a high probability that the monument pairs have different medians. Top half of each part indicates the results based on the time to reach 1 mm/yr, and the bottom half indicates the results based on b_{-2}.

indicate a lower than 10% probability that the medians are identical and the remainder are all below 50%. None of the other monument types are conclusively different from one another.

[44] There are obviously factors that could influence our observation that the deep drilled braced monuments produce the lowest noise amplitudes. These monuments only became pervasive after the initiation of the SCIGN project in 1996. Therefore the older sites had a larger mix of monuments and may suffer from increased noise (Figure 7) as a result of measurements extending further back in time. Residual common mode noise may also be a factor; sites nearer to the center of mass of the network are more likely to have lower remaining common mode noise. The positioning of monument type within the array is, however, random and so should have little influence. Each site has a particular local environment and geology that could also have an influence on noise levels. Finally, different sites are subject to varying amounts of disruption leading to the addition of noise due to offsets [*Williams*, 2003b]. These factors are again unlikely to be strongly correlated with monument type and should not influence the results. Further evidence for the lower noise amplitudes for the deep drilled braced monument comes from the BARGEN project, which consists almost exclusively of this monument type. All sites have a similar environment and a similar time span, and changes have been kept to a minimum. The median values for the north, east, and up components of the random walk amplitude are 1.0, 1.0, and 5.6 mm/yr$^{1/2}$, respectively, and the median times to reach 1 mm/yr are 0.5, 0.4, and 1.6 years. These values are better for the horizontal amplitude and slightly worse for the vertical amplitude than the results for the same monument in the SCIGN array, therefore supporting the idea that these monuments can help to increase stability. Bearing in mind the possible above influences, the evidence does appear to point to an increased stability at sites with the deep drilled braced monuments compared to the other monument types. It is also of interest that the sites situated on buildings should be ranked second in this test as intuitively we would have suspected these sites to be one of the worst. On the contrary, we would have suspected that concrete piers would have performed better, which was not the case since this type of monument ranked only better than an oil platform.

6. Discussion

[45] This study as well as previous work indicate that significant colored noise is ubiquitous in continuous GPS time series and any derived parameters and their uncertainties should take this into account.

[46] The MLE approach produces velocity and error estimates that are "most likely" in a well-defined statistical sense. Although some model for the time-dependent noise (in this work, power law noise) must be, to some extent, predefined, this is clearly preferable to the usual assumption that the noise is uncorrelated. Although the wrong assumption of the type of colored noise may give somewhat overly conservative uncertainties for the derived parameters, it is preferable to be 10% conservative than 500% optimistic [*Mao et al.*, 1999]. Furthermore, the MLE method is not susceptible to finding colored noise when there is none as shown above and by *Langbein and Johnson* [1997].

[47] *Davis et al.* [2003] claim that the MLE approach produces velocity error estimates that may be overly conservative for many sites. In the BARGEN network, *Davis et al.* [2003] used their "conservative" "whole error" method, which is equivalent to the reduced chi-square test, to determine velocity uncertainties of 0.23 mm/yr for the Northern Basin and Range (NBAR) subnetwork and 0.15 mm/yr for the Yucca Mountain cluster. From the SOPAC BARGEN solution we obtain average horizontal velocity uncertainties of 0.16 mm/yr for both subnetworks using the estimated spectral index analysis. The difference between the two approaches is that the MLE method calculates the uncertainty on a per site basis. In addition, model error is not being mixed with data error, local environments need not be the same, and also the length of time series need not be similar at all sites. The "whole error" method is simply a heuristic approach to the problem of time-correlated noise and does little to answer the two fundamental questions asked by *Davis et al.* [2003]: Are GPS velocities limited by one or more error source and if so what are those sources?. The MLE analysis presented above, hopefully, goes someway to answering these questions.

[48] The temporally correlated noise that dominates the global time series can be adequately described as flicker noise. It is spatially correlated and has a clear latitude dependence. Although the amplitude of the flicker noise has decreased in time since the first CGPS sites began producing data, it is still the dominant colored noise process in the global position time series.

[49] An issue related to the noise in the global time series is, what happens to the rate uncertainties when sites are correlated in space? Two basic strategies are employed when estimating site velocities. One is to form time series for each site from the daily solutions and then to estimate parameters from the series on a site-by-site basis. This has the advantage of being able to estimate the time-correlated noise present in the series as seen in this paper and the disadvantage of neglecting the daily spatial correlations. The other strategy is to estimate all the parameters simultaneously in some form of sequential least squares. In this approach the full covariance matrix from each day is used. If we assume that the time and space correlations are orthogonal and that the amounts of noise in the time series are similar, then it turns out that the spatial correlation between two time series propagates directly into the correlation between the parameters. The covariance of each parameter is the same as if the time series had been treated separately. This means essentially that the time series can be treated individually and the between-site correlations can be added after into a covariance matrix of site velocities. Alternatively, the spatial correlations can be accounted for in the sequential least squares to get the velocity correlations and then the velocity covariances estimated from an MLE solution to the time series. The above strategies are still good approximations even when the above assumptions are mildly violated, for example, if the two time series have slightly different ratios of flicker noise to white noise

amplitudes or if the daily spatial correlations between sites vary with time.

7. Conclusions

[50] Continuous GPS position time series from a total of 414 individual sites have been analyzed in order to assess their noise characteristics. The time series for these sites come from nine different GPS solutions, which can be broadly categorized into global and regional solutions. The regional solutions have had some form of spatially correlated signal removed from the time series in an attempt to improve the signal-to-noise ratio. The criterion for using a site was simply that it had to have more than 500 daily position estimates. The average length of time series was 1256 points and the maximum length was 3722 (over 10 years). Some sites appeared in more than one solution leading to the analysis of 954 individual time series. The maximum number of solutions in which a site appeared was five, all of which belonged to the SCIGN array in southern California. The following are the main conclusions:

[51] 1. In a global GPS solution, where no attempt has been made to reduce the spatially correlated noise, the MLE analysis indicates that a combination of white noise and flicker noise is an appropriate stochastic model for all three coordinate components. There is probably no advantage in estimating the spectral index along with the noise amplitudes considering the extra computational burden this entails.

[52] 2. The white noise amplitudes in the global solutions show a significant latitude dependence with a maximum at the equator. The flicker noise amplitudes also appear to show a latitude dependence, although not as convincingly as the white noise. For both noise components a Southern Hemisphere bias is apparent. Southern Hemisphere sites are noisier by about 1–2 mm of white noise and 2–4 mm/yr$^{1/4}$ of flicker noise.

[53] 3. There has been a significant reduction in the noise amplitudes in GPS solutions since the first continuous GPS sites began in the early 1990s. This, and the hemisphere bias, suggests that the spatially correlated noise is partly related to the reference frame and orbits. As the number of sites available for the global reference frame stabilization has increased, the noise related to it has reduced. Although the equatorial noise bulge is suggestive of a tropospheric or ionospheric origin, it may still be a feature of the reference frame via some form of error propagation.

[54] 4. In the regional GPS solutions the noise is substantially lower than in the global solutions. The actual reduction in noise depends on the areal extent, between-site distances, and number and quality of sites used to reduce the common mode noise. The larger the areal extent and baseline distances the less "common" a single common mode signal (or Helmert transformation) will be and therefore the amount removed from each individual time series will be less. The more sites used, the more representative the signal is of the regional common mode and therefore the more likely the noise is reduced.

[55] 5. Compared to the global solutions, there may be more reason to estimate the spectral index along with the noise amplitudes in the MLE algorithm. At different sites and networks, different noise sources may dominate including, for example, residual common mode noise (white noise plus flicker noise), monument instabilities (random walk noise), and localized deformation due to changes in groundwater (unknown power law noise plus annually repeating signals).

[56] 6. It is clear from Figures 2 and 4 and Table 4 that there are differences in noise content in the time series at a site between different analysis centers and different analysis strategies. For example, the white noise content in the JPL global solution is about double that in the SOPAC global solution. The flicker noise content is also larger.

[57] 7. From analysis of the SOPAC SCIGN solution the Wyatt-designed deep drilled braced monument is found to be more stable than other types of monuments, resulting in reduced noise in GPS position time series. Analyses of longer time series are required to confirm this result. However, it is premature to abandon this type of monument for the sake of less expensive solutions, in particular, with concrete pillars that performed poorly in this study.

[58] **Acknowledgments.** The authors would like to thank John Langbein, Nancy King, and Tom Herring for their careful reviews and helpful comments. We acknowledge and thank SOPAC, JPL, PANGA, REGAL, and USGS for making publicly available the position time series used in this study. This work was funded by the UK Department for Environment, Food and Rural Affairs (DEFRA), the UK Natural Environment Research Council (NERC), the U.S. National Geodetic Survey through the NOAA JIMO program, and the Southern California Integrated GPS Network (SCIGN) through the W. M. Keck Foundation, NASA, NSF, USGS, and SCEC. This research was supported by the Southern California Earthquake Center. SCEC is funded by NSF Cooperative Agreement EAR-0106924 and USGS Cooperative Agreement 02HQAG0009. SCEC contribution 759.

References

Agnew, D. (1992), The time domain behavior of power law noises, *Geophys. Res. Lett.*, *19*, 333–336.

Altamimi, Z., P. Sillard, and C. Boucher (2002), ITRF2000: A new release of the International Terrestrial Reference Frame for earth science applications, *J. Geophys. Res.*, *107*(B10), 2214, doi:10.1029/2001JB000561.

Bawden, G. W., W. Thatcher, R. S. Stein, K. W. Hudnut, and G. Peltzer (2001), Tectonic contraction across Los Angeles after removal of groundwater pumping effects, *Nature*, *412*, 812–815.

Beran, J. (1994), *Statistics for Long-Memory Processes, Monogr. Stat. Appl. Probab.*, vol. 61, 315 pp., Chapman and Hall, New York.

Bock, Y., et al. (1993), Detection of crustal deformation from the Landers earthquake sequence using continuous geodetic measurements, *Nature*, *361*, 337–340.

Bock, Y., et al. (1997), Southern California Permanent GPS Geodetic Array: Continuous measurements of the regional crustal deformation between the 1992 Landers and 1994 Northridge earthquakes, *J. Geophys. Res.*, *102*, 18,013–18,033.

Bock, Y., R. M. Nikolaidis, and M. Bevis (2000), Instantaneous geodetic positioning at medium distances with the Global Positioning System, *J. Geophys. Res.*, *105*(B12), 28,223–28,253.

Calais, E. (1999), Continuous GPS measurements across the western Alps, 1996–1998, *Geophys. J. Int.*, *138*, 221–230.

Calais, E., L. Galisson, J.-F. Stéphan, J. Delteil, J. Deverchère, C. Larroque, B. Mercier de Lépinay, M. Popoff, and M. Sosson (2000), Crustal strain in the southern Alps, 1948–1998, *Tectonophysics*, *319*, 1–17.

Davis, J. L., R. A. Bennett, and B. P. Wernicke (2003), Assessment of GPS velocity accuracy for the Basin and Range Geodetic Network (BARGEN), *Geophys. Res. Lett.*, *30*(7), 1411, doi:10.1029/2003GL016961.

Dong, D., P. Fang, Y. Bock, M. K. Cheng, and S. Miyazaki (2002), Anatomy of apparent seasonal variations from GPS-derived site position time series, *J. Geophys. Res.*, *107*(B4), 2075, doi:10.1029/2001JB000573.

Gardner, M. (1978), Mathematical games: White and brown music, fractal curves and one-over-f fluctuations, *Sci. Am.*, *238*(4), 16–32.

Granger, C., and P. Newbold (1977), *Forecasting Economic Time Series*, Academic, San Diego, Calif.

Herring, T. (2000a), Global Kalman filter VLBI and GPS analysis program, version 5.0, Mass. Inst. of Technol., Cambridge.

Herring, T. (2000b), Effects of GPS common mode errors, *Eos Trans. AGU*, *81*(19), Spring Meet. Suppl., Abstract G32A-10.

Hosking, J. R. M. (1981), Fractional differencing, *Biometrika*, *68*(1), 165–176.

Hurst, K. J., M. B. Heflin, D. Jefferson, and F. H. Webb (2000), The use of a regional reference frame in realizing the inherent precision of regional GPS, *Eos Trans. AGU*, *81*(48), Fall Meet. Suppl., Abstract G12A-01.

Johnson, H., and D. C. Agnew (1995), Monument motion and measurements of crustal velocities, *Geophys. Res. Lett.*, *22*, 2905–2908.

Johnson, H., and D. C. Agnew (2000), Correlated noise in geodetic time series, *U.S. Geol. Surv. Final Tech. Rep.*, *FTR-1434-HQ-97-GR-03155*.

Johnson, H. O., and F. K. Wyatt (1994), Geodetic network design for fault mechanics studies, *Manuscr. Geod.*, *19*, 309–323.

Journel, A. G., and C. J. Huijbregts (1978), *Mining Geostatistics*, 600 pp., Academic, San Diego, Calif.

Kedar, S., G. A. Hajj, B. D. Wilson, and M. B. Heflin (2003), The effect of the second order GPS ionospheric correction on receiver positions, *Geophys. Res. Lett.*, *30*(16), 1829, doi:10.1029/2003GL017639.

King, R., and Y. Bock (2000), Documentation for the GAMIT GPS analysis software, release 9.9, Mass. Inst. of Technol., Cambridge.

Langbein, J., and H. Johnson (1995), Noise level of geodetic monuments, *Eos Trans. AGU*, *76*(46), Fall Meet. Suppl., F142.

Langbein, J., and H. Johnson (1997), Correlated errors in geodetic time series: Implications for time-dependent deformation, *J. Geophys. Res.*, *102*, 591–603.

Mandelbrot, B. (1983), *The Fractal Geometry of Nature*, W. H. Freeman, New York.

Mandelbrot, B., and J. Van Ness (1968), Fractional Brownian motions, fractional noises, and applications, *SIAM Rev.*, *10*, 422–439.

Mao, A., C. G. A. Harrison, and T. H. Dixon (1999), Noise in GPS coordinate time series, *J. Geophys. Res.*, *104*, 2797–2816.

Miller, M. M., et al. (1998), Precise measurements help gauge Pacific Northwest's earthquake potential, *Eos Trans. AGU*, *79* (23), 269, 275.

Miller, M. M., D. J. Johnson, C. M. Rubin, H. Dragert, K. Wang, A. Qamar, and C. Goldfinger (2001), GPS-determination of along-strike variation in Cascadia margin kinematics: Implications for relative plate motion, subduction zone coupling, and permanent deformation, *Tectonics*, *20*(2), 161–176.

Nikolaidis, R. (2002), Observation of geodetic and seismic deformation with the Global Positioning System, Ph.D. thesis, Univ. of Calif., San Diego, San Diego.

Penna, N. T., and M. P. Stewart (2003), Aliased tidal signatures in continuous GPS height time series, *Geophys. Res. Lett.*, *30*(23), 2184, doi:10.1029/2003GL018828.

Press, W. H., B. P. Flannery, S. A. Teukolsky, and W. T. Vetterling (1992), *Numerical Recipes*, 818 pp., Cambridge Univ. Press, New York.

Silver, P. G., et al. (1999), A plate boundary observatory, *IRIS Newsl.*, *XVI*(2), 3–9.

vanDam, T. M., G. Blewitt, and M. B. Heflin (1994), Atmospheric pressure loading effects on the Global Positioning System coordinate determinations, *J. Geophys. Res.*, *99*, 23,939–23,950.

Watson, K. M., Y. Bock, and D. T. Sandwell (2001), Satellite interferometric observations of displacements associated with seasonal ground water in the Los Angeles basin, *J. Geophys. Res.*, *107*(B4), doi:10.1029/2001JB000470.

Wdowinski, S., Y. Bock, J. Zhang, R. Fang, and J. F. Genrich (1997), Southern California Permanent GPS Geodetic Array: Spatial filtering of daily positions for estimating coseismic and postseismic displacements induced by the 1992 Landers earthquake, *J. Geophys. Res.*, *102*(B8), 18,057–18,070.

Wernicke, B., A. M. Friedrich, N. A. Niemi, R. A. Bennett, and J. L. Davis (2000), Dynamics of plate boundary fault systems from Basin and Range Geodetic Network (BARGEN) and geologic data, *GSA Today*, *10*, 1–7.

Wilcoxon, F. (1945), Individual comparisons by ranking methods, *Biometrics*, *1*, 80–83.

Williams, S. D. P. (2003a), The effect of coloured noise on the uncertainties of rates estimated from geodetic time series, *J. Geod.*, *76*, 483–494, doi:10.1007/s00190-002-0283-4.

Williams, S. D. P. (2003b), Offsets in Global Positioning System time series, *J. Geophys. Res.*, *108*(B6), 2310, doi:10.1029/2002JB002156.

Williams, S. D. P., Y. Bock, and P. Fang (1998), Integrated satellite interferometry: Tropospheric noise, GPS estimates and implications for interferometric synthetic aperture radar products, *J. Geophys. Res.*, *103*, 27,051–27,067.

Wyatt, F. K. (1982), Displacements of surface monuments: Horizontal motion, *J. Geophys. Res.*, *87*, 979–989.

Wyatt, F. K. (1989), Displacements of surface monuments: Vertical motion, *J. Geophys. Res.*, *94*, 1655–1664.

Wyatt, F. K., H. Bolton, S. Bralla, and D. C. Agnew (1989), New designs of geodetic monuments for use with GPS, *Eos Trans. AGU*, *70*, 1054.

Zhang, J. (1996), Continuous GPS measurements of crustal deformation in southern California, Ph.D. dissertation, Univ. of Calif., San Diego.

Zhang, J., Y. Bock, H. Johnson, P. Fang, S. Williams, J. Genrich, S. Wdowinski, and J. Behr (1997), Southern California Permanent GPS Geodetic Array: Error analysis of daily position estimates and site velocities, *J. Geophys. Res.*, *102*(B8), 18,035–18,055.

Zumberge, J. F., M. B. Heflin, D. C. Jefferson, M. M. Watkins, and F. H. Webb (1997), Precise point positioning for the efficient and robust analysis of GPS data from large networks, *J. Geophys. Res.*, *102*, 5005–5017.

Y. Bock, P. Fang, P. Jamason, R. M. Nikolaidis, and L. Prawirodirdjo, Cecil H. and Ida M. Green Institute of Geophysics and Planetary Physics, Scripps Institution of Oceanography, 9500 Gilman Drive, La Jolla, CA 92093-0225, USA. (ybock@ucsd.edu; pfang@ucsd.edu; pjamason@ucsd.edu; rosanne@ucsd.edu; linette@josh.ucsd.edu)

D. J. Johnson, Department of Earth and Space Sciences, University of Washington, Seattle, WA 98115, USA. (dj@ess.washington.edu)

M. Miller, Department of Geology, Central Washington University, 400 E 8th Avenue, Ellensburg, WA 98926-7418, USA. (meghan@geology.cwu.edu)

S. D. P. Williams, Proudman Oceanographic Laboratory, Bidston Observatory, Bidston CH43 7RA, UK. (sdwil@pol.ac.uk)